blast-like stem/progenitor cells can be converted into myocytes by tamoxifen-induced MYOD-ER overexpression [13]. Goudenege et al. also showed that hiPSC-derived mesenchymal cells can be promoted to myogenic differentiation efficiently by Adenoviral-transduction mediated *MYOD1* overexpression [14]. The 2 reports both indicated that iPSC-derived mesodermal or mesenchymal cells, both of which are differentiated for more than 2 weeks from undifferentiated hiPSCs, have a high potential for myogenic differentiation in response to *MYOD1* overexpression. However, such differentiation steps prior to *MYOD1* transduction might contribute to the reported observation of low reproducibility. Because mouse embryonic stem cells (mESCs) are able to directly differentiate to myocytes in response to Tetracycline (Tet)-induced *MYOD1* expression [15], we assessed whether drug-induced *MYOD1* expression could similarly promote efficient myocyte differentiation directly from undifferentiated hiPSCs. Here, we demonstrate that *MYOD1* overexpression in immature hiPSCs drives them to mature as myocytes with very high efficiency and reproducibility within 2 weeks.

Miyoshi myopathy [16] (MM) is a congenital distal myopathy caused by defective muscle membrane repair as a result of mutations in DYSFERLIN [17,18]. Research directed at understanding the MM pathology has been primarily performed using model mice. To evaluate the true pathology of human disease, it is important to exploit current iPSC technology for direct assessment of patient samples. Here, we apply our differentiation technique to MM-disease modeling, recapitulating disease pathology *in vitro*, and successfully rescue the phenotype of MM by gene repair. The differentiation method presented here is suitable for muscular disease modeling by using patient-derived hiPSC. Our method of MYOD1-induced myogenic differentiation directly from undifferentiated hiPSCs is also suitable for the establishment of drug screening systems by using patient-derived hiPSCs. This is due to the unlimited proliferation potential of hiPSCs and uniformity in the undifferentiated state, which may prevent variation in differentiation frequency.

Results

Generation of hiPSCs with Drug-inducible *MYOD1* Expression

We constructed a self-contained, drug-inducible expression vector, based on the *piggyBac* (PB) transposon [19]. This vector constitutively expresses the neomycin (G418) resistance gene along with the rtTA transactivator element, which mediates doxycycline (Dox)-dependent activation of cDNA cassettes controlled by tetO promoter (PB-TAC-ERN; **Fig. 1a**). Activation of gene expression in response to Dox may be indirectly monitored by co-incident mCherry activation. Using Gateway cloning, we produced a derivative vector containing the human *MYOD1* gene (Tet-MyoD1). The Tet-MyoD1 vector was transfected together with PB transposase (PBase) into 3 independent hiPSC lines, and selected in G418 supplemented media for 5 days to generate pooled MyoD-hiPSCs containing genomic transposon integrations (**Fig. 1b**). In these pooled MyoD-hiPSCs, Dox administration for 24 h robustly induced *MYOD1* expression as detected by mCherry fluorescence and MYOD1 protein (**Fig. 1c**). As some cells did not express mCherry, we selected appropriate MyoD-hiPSC clones with robust, uniform levels of mCherry induction for further analysis. These clones retained pluripotency, which was confirmed by their expression of surface markers (**Fig. S1a**) and gene characteristic of an undifferentiated state (**Fig. S1b**), as well as teratoma formation (**Fig. S1c**). These clones were selected by the high expression of mCherry after Dox administration (**Fig. S2a**). RT-PCR analysis of these clones confirmed undetectable exogenous *MYOD1* background expression in the absence of Dox, whereas Dox treatment strongly induced exogenous *MYOD1* within 48 h, in correlation with mCherry expression (d2). Importantly, despite continued maintenance in hiPSC culture conditions, endogenous *MYOD1* activation was detectable after 96 h (d5) of Dox induction, with the effect being reproducible in MyoD-hiPSC clones derived from 3 distinct hiPSC lines: 201B7, 253G1, and 254G4 [1] (**Fig. S2b**). In selected MyoD-hiPSC clones, mCherry expression was detected uniformly 24 h after Dox administration in hiPSC-maintenance conditions (**Fig. 1d**). When the addition of Dox was continued for 7 days under hiPSC-maintenance conditions, the emergence of myosin heavy chain (MHC) [20] positive cells was extremely limited to the edge of MyoD-hiPSC colonies, and many MyoD-hiPSCs lines retaining undifferentiated colonies (**Fig. 1d**). On the other hand, when the culture medium was exchanged for differentiation medium on d1, MyoD-hiPSCs were differentiated into MHC positive myocytes disrupting colony formation. This medium replacement resulted in highly efficient myogenic induction (**Fig. 1e**). These results suggest that extended expression of transgenic *MYOD1* was able to activate the myogenic differentiation program in undifferentiated hiPSCs, even under sub-optimal conditions.

Dox-induced Myogenic Differentiation of MyoD-hiPSCs

As MyoD-hiPSCs maintained an undifferentiated status in hiPSC maintenance medium (**Fig. 1d**), we sought to optimize the differentiation protocol by adjusting culture conditions to be more appropriate for myogenic induction; first removing basic-fibroblast growth factor (b-FGF) for spontaneous differentiation, and then changing to alpha Minimal Essential Medium (αMEM) supplemented with a low concentration (5%) of knockout serum replacement (KSR). Dox treatment was maintained throughout the analysis. Early medium replacement to low-KSR αMEM enhanced myogenic differentiation, whereas late replacement did not improve differentiation compared to continued culture in hiPSC maintenance media without bFGF (**Fig. 2a**). Media containing a low concentration of horse serum has been shown to promote the maturation of myoblast into myotubes [9,21]. To examine this later stage of differentiation, we assessed the effect of serum on the maturation of Dox-induced myogenic cells by counting the number of nuclei per myotube on d9. Although the difference was not statistically significant, a tendency towards higher numbers of nuclei was detected in hiPSCs cultured in 5% horse serum as compared to 5% KSR (**Fig. 2b**).

We predicted that the initiation point and period of Dox administration could also have an effect on differentiation responses. Dox addition at day 1 (d1) of differentiation (24 h after bFGF removal) induced over 90% mCherry positive cells. However, Dox addition later on in the differentiation protocol (d4) revealed an unresponsive, mCherry negative population (**Fig. 2c, d**), suggesting a failure of the expression vector to activate in a proportion of partially differentiated cells. To assess whether fully differentiated hiPSCs can be promoted into myogenic differentiation by Dox-mediated *MYOD1* expression, we applied our system to mesenchymal progenitor cells, known as SB-outgrowth cells (SB-OGs) [5], derived from hiPSCs. According to the report of Mahmood et al, SB-OGs derived from MyoD-hiPSCs were established after 14 days of differentiation, and were passaged twice [5]. When Dox was administrated to SB-OGs cultures, low levels of mCherry expression were observed, indicating low myogenic differentiation efficiency (**Fig. S3a, b**). Taken together, these results indicate that our inducible gene expression system using the *piggyBac* vector is suitable for driving

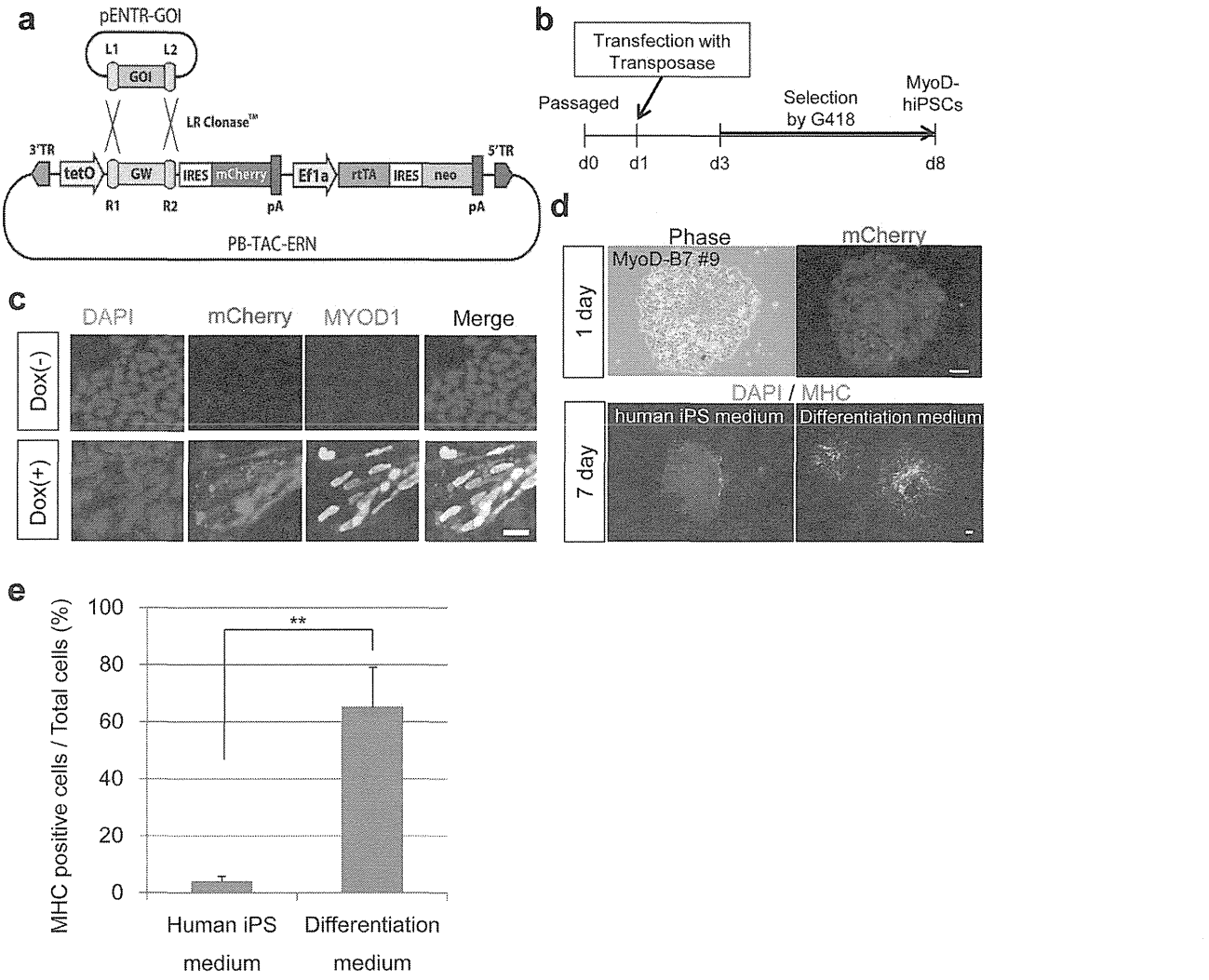

Figure 1. Generation of MyoD-hiPSCs. (**a**) Construction of the Tet-inducible *MYOD1* expressing *piggyBac* vector (Tet-MyoD1 vector). (**b**) A scheme of generation of MyoD-hiPSCs. Human iPSCs were transfected the Tet-MyoD1 vectors with transposase by lipofection. To select transfected cells, G418 were added for 5 days in the hiPSC culture media at 2 days after transfection. (**c**) MyoD-hiPSCs after 24 h in culture with or without Dox administration. Scale bar = 20 μm. (**d**) Upper lanes show dox-added MyoD-hiPSCs at d1. Lower lanes show immunodetection of MHC in Dox-induced MyoD-hiPSCs at d7. A lower-left panel shows the cells differentiated in maintenance medium from d1 to d7. A lower-right panel shows the cells differentiated in αMEM containing 5% KSR from d1 to d7. Scale bars = 200 μm. (**e**) Percentage of MHC positive cells per total cells following MyoD-induced differentiation. $^{**}p<0.01$.
doi:10.1371/journal.pone.0061540.g001

the expression of genes in undifferentiated hiPSCs, rather than those which have been differentiated. However, Dox administration at the initiation of differentiation (d0; coincident with the change to low-serum media) led to lower cell survival (data not shown). Therefore, Dox administration was initiated at the fixed time point, d1, in our system. Next, we examined the period of Dox administration. MyoD-hiPSCs did not differentiate into myocytes following less than 3 days of Dox administration (**Fig. 2e**). Beyond 5 days of administration, continued Dox treatment did not significantly enhance the induction of MHC positive myocytes (**Fig. 2e**), revealing that 5–6 days of Dox administration was sufficient to commit MyoD-hiPSCs to a myogenic lineage. Next, we investigated the effect of initiating Dox administration on various days. Although Dox administration on d0 resulted in a large amount of cell deaths, early Dox administration resulted in highly efficient differentiation (**Fig. S3c, d**). Using these optimized parameters, we established a standardized protocol for myogenic differentiation of MyoD-hiPSCs (**Fig. 3a**).

Applying this differentiation protocol, all MyoD-hiPSC clones derived from 3 distinct parental hiPSC lines could be promoted to form MHC positive myotubes (**Fig. 3b**). The efficiency was calculated from the percentage of MHC positive cells among total cells, and consistently ranged from 70% to 90%, irrespective of the clone of origin (**Fig. 3c**). Differentiated MyoD-hiPSCs changed their shape to spindle-like, uniformly (**Movie S1**). Thus, dominant drug-regulated expression of exogenous *MYOD1*, combined with our differentiation culture conditions overcomes clonal variation, and actualizes efficient and uniform myogenic differentiation.

Differentiation of Myocytes from MyoD-hiPSCs Occurs Directly

To characterize cell responses to this updated differentiation protocol, we analyzed the time course of gene expression of both

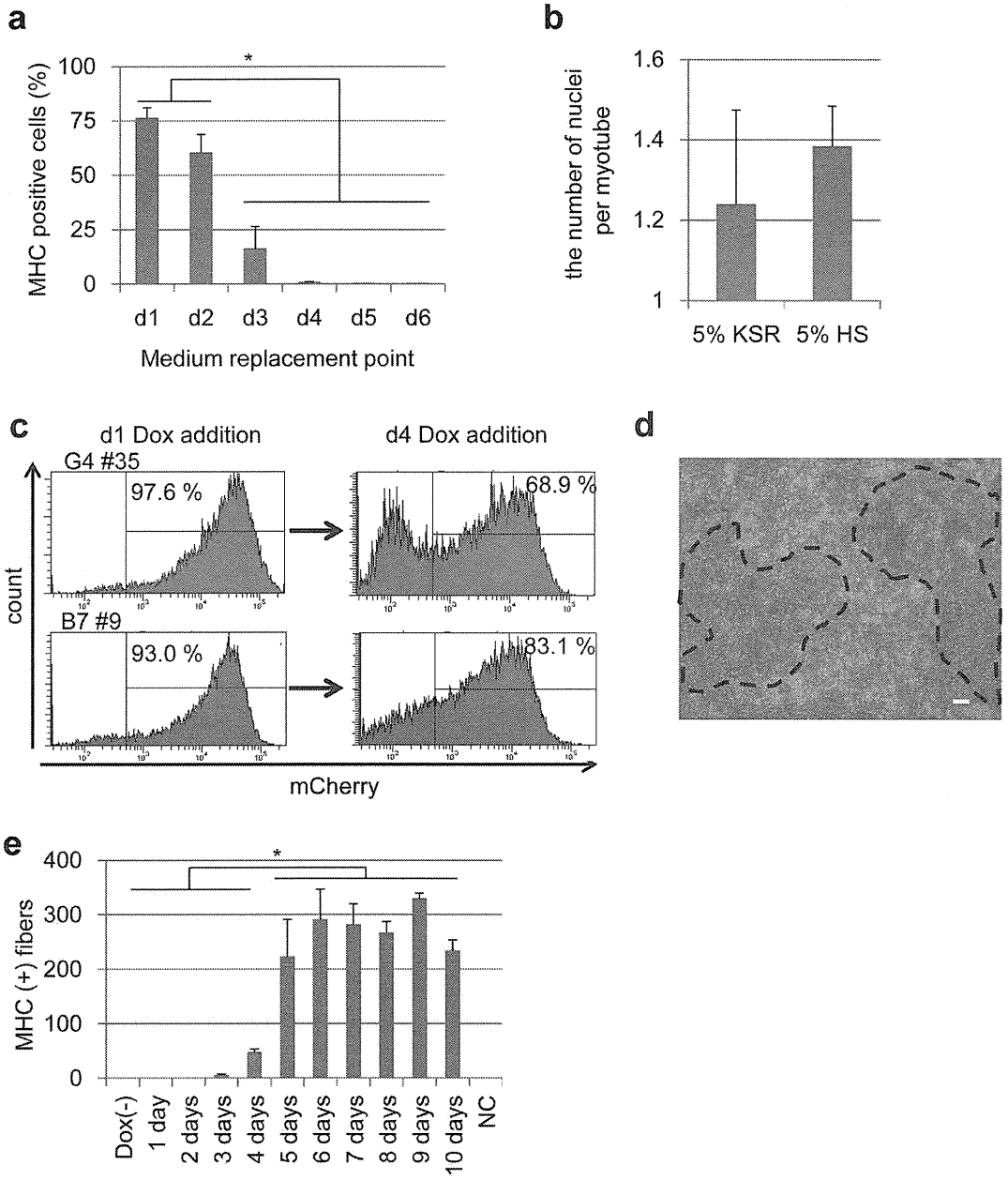

Figure 2. Optimization of Differentiation Conditions. (**a**) Percentage of MHC positive myogenic cells derived from MyoD-hiPSCs during 9 days differentiation with various timing of medium replacement. *$p<0.05$ (**b**) The average number of nuclei of myofibers in each condition of 5% KSR or 5% HS containing media after 7 days differentiation. (**c**) Flow cytometric analysis of MyoD-hiPSCs with 24 h Dox treatment in different start points. Dox addition at differentiation d1 promoted higher percentage of mCherry expression in MyoD-hiPSCs than Dox addition at differentiation d4. (**d**) A merged image of phase-contrast and mCherry images in differentiated MyoD-hiPSCs which were administrated Dox at differentiation d4. Some MyoD-hiPSCs turned to be unresponsive with Dox, indicating no mCherry expression area (dotted line). Scale bar = 100 μm. (**e**) MHC positive myogenic cell number derived from MyoD-hiPSCs during 11 days differentiation with various administration periods of Dox. *$p<0.05$.
doi:10.1371/journal.pone.0061540.g002

undifferentiated and myogenic markers in the presence or absence of Dox (**Fig. 4a**). Expression of mCherry, synonymous with exogenous *MYOD1* expression, was the highest at d2 and declined throughout the protocol. As expected, the expression of markers of the undifferentiated markers [22], such as *OCT3/4*, *SOX2* and *NANOG*, gradually decreased through the course of differentiation (**Fig. 4a, gray bars**). The expression of endogenous *MYOD1* and *MYOGENIN* [23], both of which are directly and positively regulated by MYOD1, appeared at d3 and peaked at d7 (**Fig. 4a, gray bars**). Furthermore, mature myofiber markers such as *creatine kinase muscle isoform* (*CK-M*) [24] and *DYSTROPHIN (DMD)* [25], were also detected following exogenous *MYOD1* expression (**Fig. 4a, gray bars**). By contrast, prolonged expression of genes characteristic lacking differentiation and an absence of myogenic gene expression were observed in the absence of Dox administration (**Fig. 4a, black bars**). Similar to observations in mouse ESCs [15], Dox-induced *MYOD1* expression in hiPSCs is sufficiently potent to directly promote myogenic differentiation, even in completely undifferentiated cells. In development, myogenic cells derive from a progenitor of mesodermal origin.

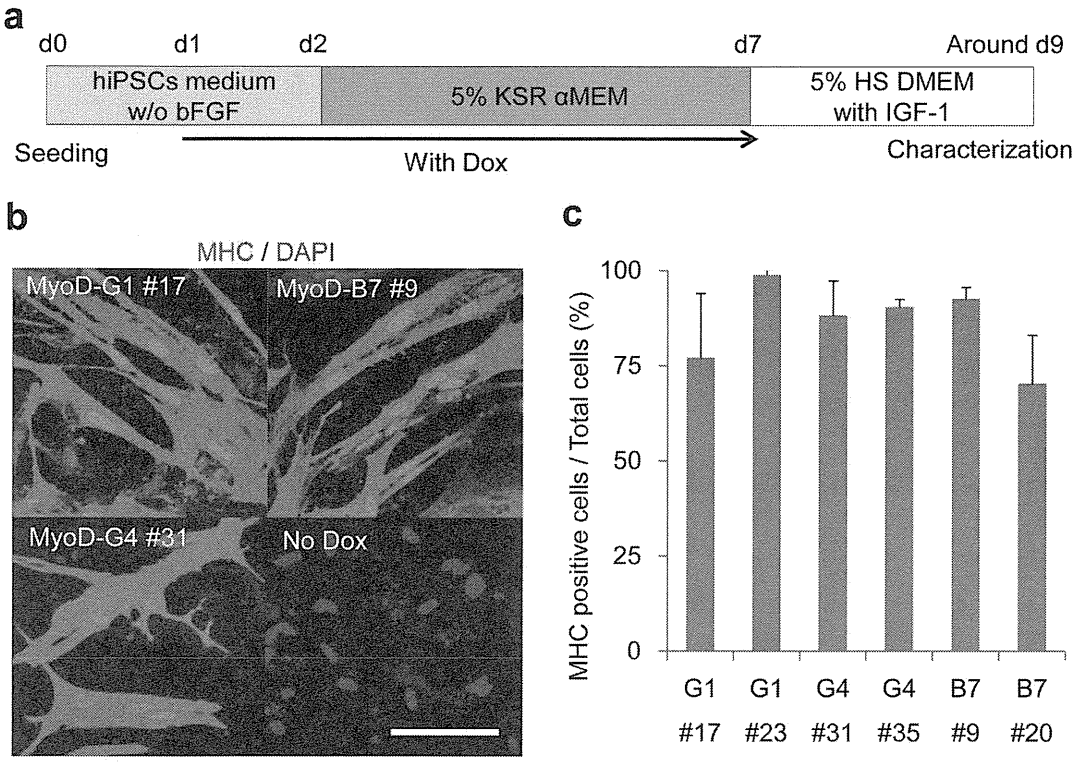

Figure 3. Reproducible myogenic differentiation with the optimized protocol. (**a**) A schematic of our muscle differentiation protocol beginning with MyoD-hiPSCs. (**b**) Immunohistochemistry of differentiated MyoD-hiPSCs for MHC (red). Scale bar = 100 μm. (**c**) Percentage of MHC positive cells per total cells following MyoD-induced differentiation of 6 MyoD-hiPSC clones. (n = 3 for each clone). Data are listed as mean ±S.D.
doi:10.1371/journal.pone.0061540.g003

To further assess whether Dox-induced myogenic differentiation proceeded *via* mesodermal differentiation, expression of mesodermal marker genes was analyzed. The pan-mesodermal marker *BRACHYURY* (*T*) [26], paraxial mesodermal markers *MESP2* [27] and *TBX6* [28], and a dermomyotome marker *PAX3* [29] were expressed transiently during Dox-induced differentiation, whereas in the absence of Dox very low expression of mesodermal genes was observed (**Fig. S4**). To determine whether mesodermal gene expression is essential for myogenic differentiation in our system, siRNA was used to suppress *T* or *TBX6* during the early phase of differentiation. Expression of *T* or *TBX6* was strongly suppressed on d3 and d5 by 48 h of pretreatment with siRNA (**Fig. S5a, b**). Furthermore, both *T* and *TBX6* siRNA treatments indirectly suppressed expression of *PAX3*, which is upstream of *MYOD1* [30]. Despite suppression of mesodermal gene expression, efficiencies of myogenic differentiation were not affected (**Fig. S5c, d**). Thus, although several mesodermal genes express transiently, MyoD-hiPSCs successfully differentiate along a myogenic lineage independent of these factors, seemingly circumventing a mesodermal intermediate stage.

Myocytes Derived from MyoD-hiPSCs Resemble Mature Myocytes *in vivo*

To assess myogenic properties of differentiated MyoD-hiPSCs, histological and gene expression analyses were performed. Although undifferentiated hiPSCs had few mitochondria, differentiated MyoD-hiPSCs had many mitochondria surrounding their nuclei (**Fig. 4b**). Furthermore, differentiated MyoD-hiPSCs expressed the mature myocyte markers, DYSTROPHIN, skeletal muscle Actin and CK-M (**Fig. 4c**). Skeletal muscle Actin does not appear in cardiac muscle and is therefore used to distinguish skeletal myocytes from cardiomyocytes. These features suggest that Dox-induced myogenic cells derived from MyoD-hiPSCs have characteristics of mature myocytes. To further define myogenic cell identity, we analyzed global gene expression profiles of differentiated MyoD-hiPSCs, comparing these with the differentiated immortal human myoblast cell line Hu5/E18 [31,32], and undifferentiated hiPSCs (**Fig. 4d, e**). The microarray profiles of differentiated MyoD-hiPSCs were similar to those of differentiated Hu5/E18 and quite divergent from those of undifferentiated hiPSCs (**Fig. 4d**). Multiscale bootstrap clustering analysis showed that MyoD-hiPSCs derived myocytes had statistically significant different gene expression profiles from those of undifferentiated hiPSCs and similar gene expression profiles to those of Hu5/E18 derived myocytes (**Fig. S6**). Furthermore, we selected specific genes associated with muscle differentiation and analyzed mRNA expression profiles. Differentiated MyoD-hiPSCs showed high expression levels of the selected muscle associated genes, similar to differentiated Hu5/E18 cells (**Fig. 4e**), with the exception of *MYF5* [33], an upstream transcription factor regulating *MYOD1* (**Fig. 4e**). These data were confirmed by quantitative real time PCR. Consistent with the results of microarray analysis, myogenic transcription factors such as *MYOD1*, *MYOGENIN*, *MEF2C* [34] and *SIX1* [35], which are downstream genes of *MYOD1*, were upregulated in induced cells but not in undifferentiated cells. By contrast, *MYF5*, which is an upstream gene of *MYOD1*, was not upregulated in induced cells (**Fig. S7**). Taken together, Dox-induced myogenic cells generated from MyoD-hiPSCs appear to represent mature myocytes similar to differentiated human myoblasts. Yet, unlike human myoblasts, MyoD-hiPSCs do not express *MYF5*, and may transit directly from undifferentiated into *MYOD1* positive myogenic cells.

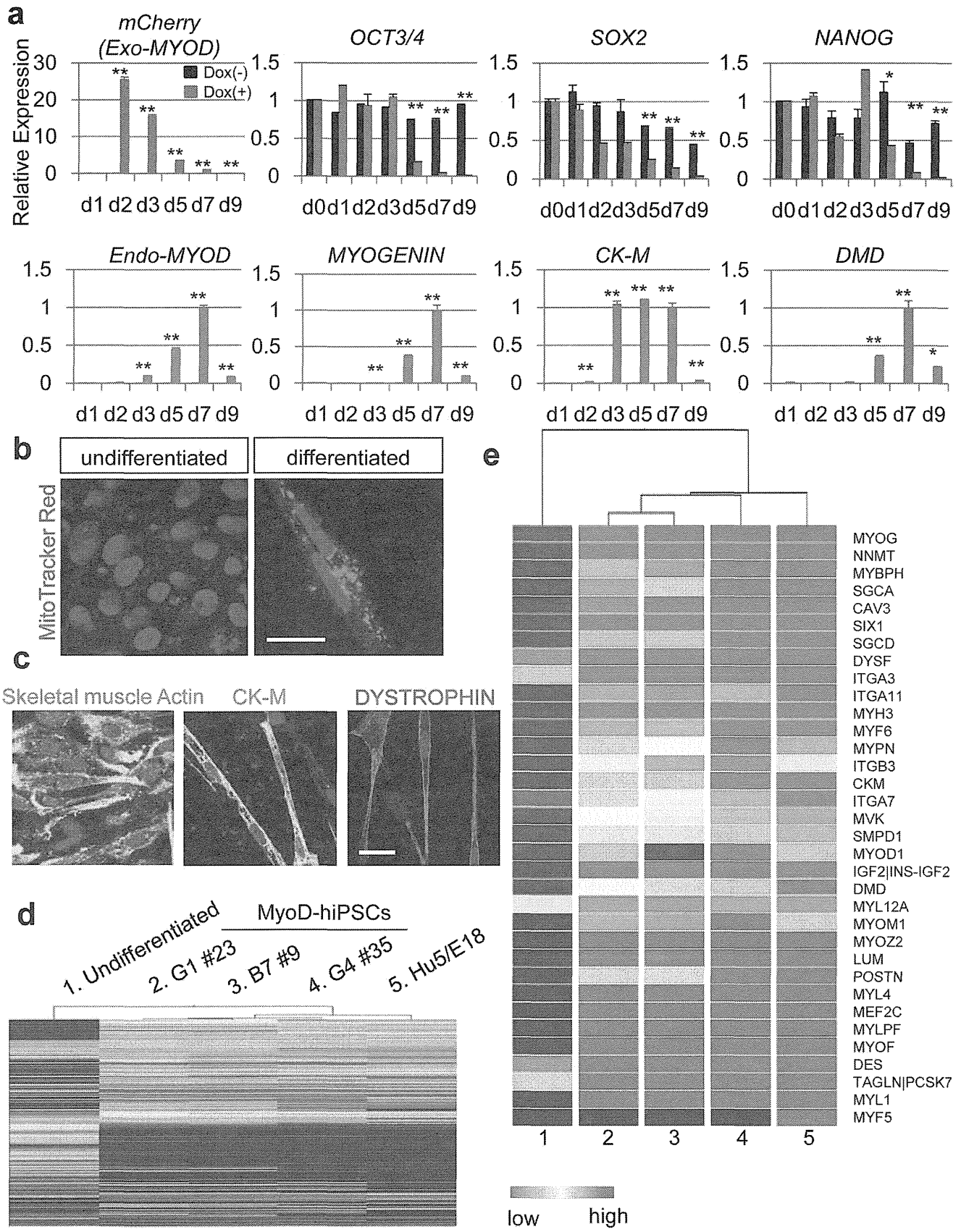

Figure 4. Characterization of myofiber derived from MyoD-hiPSCs. (**a**) Time course gene expression profile for undifferentiated and myogenic markers in B7 #9 MyoD-hiPSC clone with (gray bars) or without (black bars) Dox administration (n = 3). Data are listed as mean±S.D. The

data were standardized by β-actin using teratoma. The data on d0 = 1 in undifferentiated markers, such as *OCT3/4, SOX2* and *NANOG*. The data on d7 = 1 in other analyses. *: $p<0.05$, **: $p<0.01$, respectively, between Dox(–) and Dox(+). (**b**) Intracellular localization of mitochondria in both undifferentiated and differentiated MyoD-hiPSCs. Scale bar = 20 μm. (**c**) Immunohistochemistry of differentiated MyoD-hiPSCs for mature myogenic markers, such as CK-M, creatine kinase muscle isoform, Skeletal muscle Actin, and DYSTROPHIN. Scale bar = 20 μm. (**d**) Heat map of global mRNA expression comparing undifferentiated hiPSC (sample 1) and differentiated myogenic cells (samples 2-5). (**e**) Myogenic gene profile and unsupervised clustering based on markers associated with myofibers for undifferentiated hiPSCs and differentiated myogenic cells. Red color indicates up-regulated genes and blue color indicates down-regulated genes in (**d**) and (**e**).
doi:10.1371/journal.pone.0061540.g004

Functional Properties of Dox-induced Myocytes Derived from MyoD-hiPSC

Structural analysis by electron microscopy revealed that differentiated MyoD-hiPSCs have myofibrils containing future Z line-like structures, and myosin fibers similar to differentiated Hu5/E18 (compare **Fig. 5a, b**). To assess whether such structural properties are sufficient to mediate contraction, Dox-induced myogenic cells were electrically stimulated. As predicted, *MYOD1* induced myotubes could contract coincident with electrical pulses (**Movie S2**). Another discriminating characteristic of myogenic cells is cell fusion, leading to multi-nucleated myotubes. With regard to fusion potential, differentiated MyoD-hiPSCs were co-cultured with the mouse myoblast cell line C2C12 [21], engineered to express GFP. MyoD-hiPSCs were induced towards myogenic differentiation for 7 days. On d7, C2C12 cells were seeded onto induced MyoD-hiPSCs. Two days after co-culture, mCherry positive human myogenic cells fused with GFP positive murine myogenic cells were identified by time lapse photography (**Fig. 5c** and **Movie S3**). Several days later, immunohistochemistry revealed that a number of human nuclei in murine myotubes, confirming cell fusion *in vitro* (**Fig. 5d**). Finally, we transplanted differentiated MyoD-hiPSCs into tibialis anterior muscles (TA muscle) of non-obese diabetic/severe-combined immunodeficient-duchenne muscular dystrophy null (NOD/scid-DMD) mice [36] (**Methods**). On d28 after transplantation, although the number of signals was a few, specific staining with anti-human spectrin (**Fig. S8a**) and anti-human dystrophin (**Fig. S8b**) was detected in mouse TA muscles. These results indicate that MyoD-hiPSC-derived myocytes display fusion potential both *in vitro* and *in vivo*. Taken together, Dox-induced myogenic cells derived from MyoD-hiPSCs achieve the functional properties of muscle, similar to differentiated human myoblasts.

Application of Myogenic Differentiation to Disease Modeling

We applied our myogenic induction system to assess the utility of these differentiated cells in modeling the human disease Miyoshi myopathy (MM) [16]. MM hiPSCs were generated from MM patient fibroblasts by transduction of the 4 Yamanaka factors (*OCT4*, *SOX2*, *KLF4* and c-*MYC*) with Sendai virus (SeV) vectors (**Methods**). Subsequently, we introduced the Tet-MyoD1 vector into MM hiPSCs, and chose 2 independent clones (MyoD-MM #5 and #6) for further analysis. These 2 clones were morphologically identical to the other hiPSCs (**Fig. 6a**), expressed endogenous pluripotency marker genes without detectable persistence of the SeV viral RNA genome (**Fig. 6b**), and formed teratomas *in vivo* (**Fig. S9**). MyoD-MM hiPSCs were unhindered in their ability to differentiate into MHC or MYOGENIN positive mature myocytes (**Fig. 6c**). Yet, differentiated MyoD-MM cells demonstrated impaired expression of DYSFERLIN [17,18], as expected from the primary genetic lesion (**Fig. 6d, lanes 1, 2**). Thus, we derived rescued MyoD-MM+Dysf hiPSC clones by stable transgenic over-expression of DYSFERLIN, and confirmed DYSFERLIN expression in 2 rescue clones and the MyoD-B7 #9 control line by western blotting (**Fig. 6d**).

To recreate pathological conditions, we assessed membrane repair function in both diseased and DYSFERLIN-rescued MyoD-MM hiPSCs compared to control MyoD-hiPSCs (**Fig. 6e, f**). A myotube from MyoD-MM clone #5 displayed extensive uptake of FM1-43 in all cytoplasmic lesions, indicating defective membrane repair following two-photon laser-induced injury of the sarcolemma [17] (**Fig. 6e left**, **Movie S4**). In contrast, myotubes from MyoD-MM #5+ Dysf and MyoD-B7 #9 control cells display focal uptake of FM1-43 at the damaged area (**Fig. 6e center and right panels, Movie S5 and S6**). Indeed, the apparently unimpeded uptake of FM1-43 observed in MM patient-derived myotubes, was reversed by over-expression of *DYSF*, suggesting efficient membrane resealing, similar to control cells (**Fig. 6f**). Thus, in vitro differentiated MM patient iPSCs faithfully recapitulated the expected pathological condition, which could be reversed by overexpression of the affected gene product, suggesting a possible treatment for MM by using gene therapy.

Discussion

Over the years, engineered model mice have been the mainstay in understanding disease pathology [36,37,38]. Yet, due to discrepancies between mouse phenotypes and actual human disease pathology [39], it would be preferable to evaluate disease and perform *in vitro* screening for potential therapeutics in a reliable human system. In considering *in vitro* disease modeling and screening, large numbers of cells are necessary to generate and reproduce experimental data. Fibroblasts and many other somatic cells are not able to proliferate indefinitely and quickly reach senescence, failing to maintain a similar level of quality throughout their limited replicative lifespan. As hiPSCs have a clear advantage as an indefinitely self-renewing cell source for *in vitro* assays, iPSC technology coupled with robust *in vitro* differentiation has been hailed as a major breakthrough in the field [40]. Myogenic induction from hiPSCs, following the protocols outlined here, provides consistent quality, exhibiting higher efficiency and reproducibility than described in previous reports [10,12], whereas the period required for induction is as short as 10 days. These are significant improvements and represent major steps towards iPSC-based disease-modeling and drug screening for myogenic disorders.

Although forced expression of *MYOD1* by mRNA treatment can induce myocytes from hiPSCs-derived fibroblasts, the efficiency of myogenic differentiation is limited to less than 40% [12]. This may in part be due to a low efficiency of mRNA transfection in fibroblasts. In contrast, the *piggyBac* vector system employed here presents advantages in obtaining transgenic hiPSCs through efficient and stable genomic integration, a suitable approach for *in vitro* applications. Transgenic hiPSC populations or clones carrying the *piggyBac* vector may be easily purified before Dox induction by using simple drug selection. Clones derived in this manner display robust and uniform drug-induced transgene activation through the early stages of differentiation, ensuring an effective and coordinated response, and thus achieving efficiencies in excess of 70%. Furthermore, the *piggyBac* Tet-inducible gene expressing vector is almost completely inactive in partially or fully

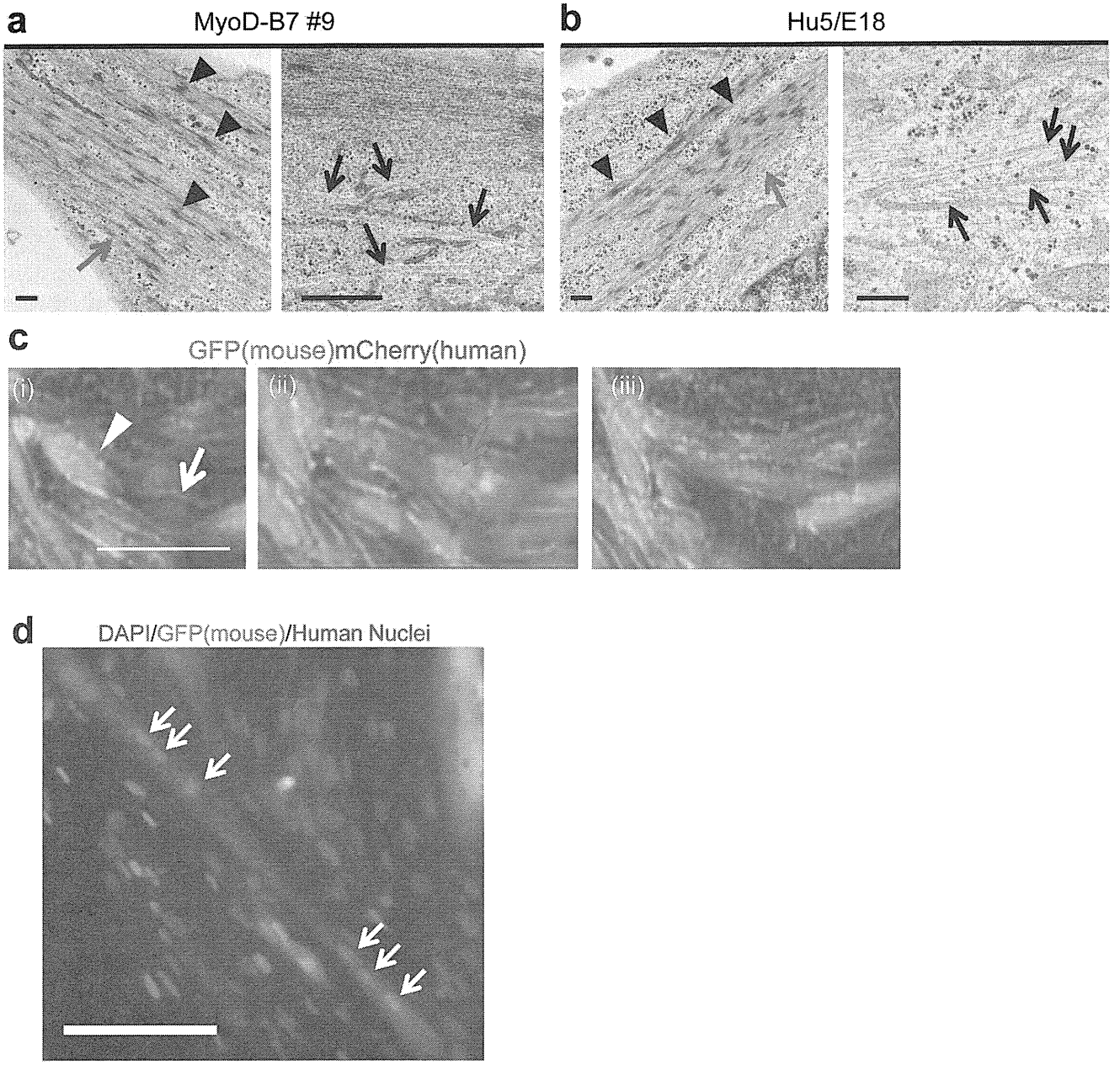

Figure 5. Functional assay for differentiated MyoD-hiPSCs. (**a, b**) Electron microscopy of differentiated MyoD-hiPSCs (**a**) and differentiated human myoblast Hu5/E18 cells (**b**). Red arrows indicate myofibrils. Black arrowheads indicate future Z lines. Black arrows indicate myosin fibers. Scale bars = 500 nm. (**c**) Serial photographs of differentiated MyoD-hiPSCs co-cultured with C2C12 cells. A hiPSC-derived mCherry+ cell (white arrow) fused with a mouse-derived GFP+ cell (white arrowhead) resulting in a yellow cell (red arrow). Time increments between images = TIME. Scale bar = 100 μm. (**d**) Immunohistochemistry of MyoD-hiPSCs co-cultured with C2C12 cells. White arrows indicate human nuclei in a GFP+ murine myofiber. Scale bar = 100 μm.
doi:10.1371/journal.pone.0061540.g005

differentiated hiPSCs, but expresses strongly in undifferentiated hiPSCs. By initiating differentiation using the master regulator, MYOD1, in homogenous undifferentiated hiPSCs, rather than a heterogenous differentiated cell population, our approach achieves highly consistent efficiency. Recently, several reports have demonstrated highly efficient myogenic differentiation of hiPSCs driven by the overexpression of transcription factors [6,13,14]. Darabi et al. showed that PAX7-overexpression in mesodermal cells differentiated from hiPSCs through embryoid body formation, could promote efficient myogenic differentiation and generate transplantable myogenic progenitors which were applicable for muscle regeneration. However, their method of differentiation entailed many complicated steps including cell sorting by flow cytometer, and the time taken to induce mature myocytes was more than 4 weeks [6]. Tedesco et al. demonstrated that human iPSC-derived mesoangioblast-like progenitors (HIDEMs) could be generated by a 3 weeks, multi-step differentiation method. Although, the HIDEMs were able to act as transplantable myogenic progenitors, with excellent regeneration potentials in impaired muscle, they had poor myogenic

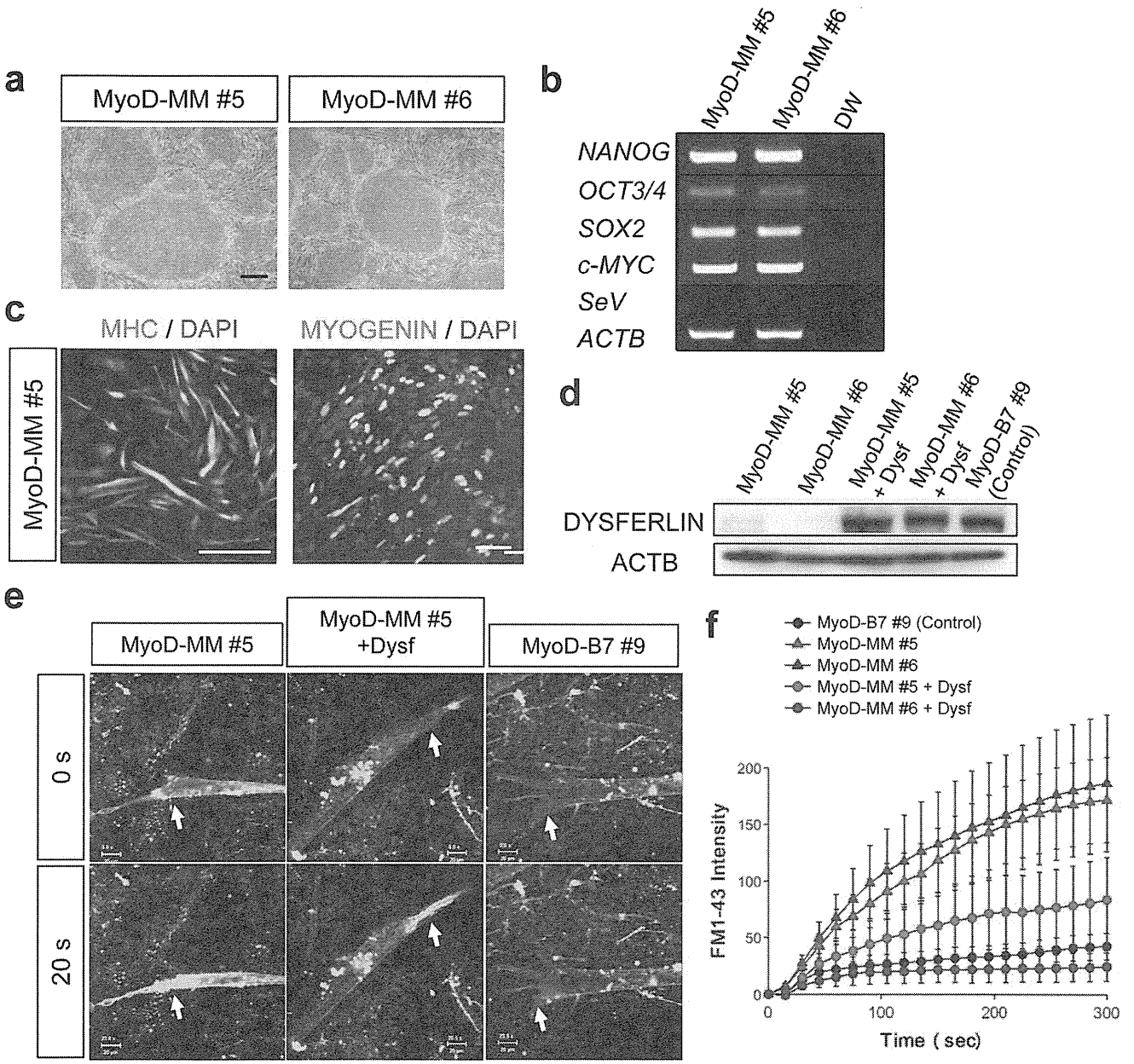

Figure 6. Modeling Miyoshi Myopathy (MM) by patient derived-hiPSCs. (**a**) Morphology of patient derived MM-hiPSC clones, expanded following G418 selection for Tet-MyoD1 vector transposition. Scale bar = 200 μm. (**b**) RT-PCR analysis of endogenous pluripotent stem cell markers in MyoD-MM hiPSCs. (**c**) Efficient myogenic differentiation of MyoD-MM hiPSCs according to the protocol defined in Figure 3a. MHC positive (left), or Myogenin positive (right) cells were observed dominantly. Scale bars = 100 μm. (**d**) DYSFERLIN expression of the myofibers from MyoD-MM hiPSCs (lane 1, 2), rescued MyoD-MM hiPSCs which expressed full-length *DYSF* cDNA driven by EF1α promoter (lane 3, 4), and control non-diseased MyoD-hiPSCs (lane 5) confirmed by western blotting. ACTB = β-actin. (**e**) Entry of FM1-43 green fluorescent dye into differentiated myofibers from MyoD-MM #5 (left), rescued MyoD-MM #5 with *DYSF* expression (middle), or control MyoD-hiPSC clone B7 #9 (right), before (0 s) and 20 s after (20 s) two photon laser-induced damage of the sarcolemmal membrane (arrow). Scale bars = 20 μm. (**f**) Summary time course data of accumulation of FM1-43 dye in laser-damaged myofibers derived from B7 #9 (black circles), MyoD-MM hiPSCs (red or blue triangles) and rescued MyoD-hiPSCs with DYSFERLIN expression (red or blue circles). n = 5 for each clone. Data are listed as mean ±S.E.
doi:10.1371/journal.pone.0061540.g006

differentiation potential *in vitro*; efficient *in vitro* myogenic induction of the HIDEMs depended on forced expression of *MYOD1* from a tamoxifen-inducible lenti-viral vector system [13]. Goudenege et al. demonstrated that efficient myogenic differentiation could be induced from hiPSC-derived mesenchymal cells by adeno-viral transduction of *MYOD1* [14]. The use of an integration-free adenoviral system could be advantageous for muscular disease cell therapy, but it could potentially be a complicated step during establishment of drug screening platforms following disease modeling. In all 3 previously reported procedures, hiPSCs were differentiated into mesodermal or mesenchymal progenitors prior to forced expression of the transcription factors. Although, these procedures able to induce myogenic progenitors for use in cell therapy, pre-differentiation steps, with serum-containing medium, could increase the clonal variation of hiPSCs, and consequently affect the reproducibility of

the methods. By contrast, we initiated differentiation in undifferentiated hiPSCs, which are relatively homogenous, and our simple method exhibits high reproducibility. Therefore, our method has advantages for application in drug screening following muscular disease modeling by using patient-derived hiPSCs, as a simple, rapid, and reproducible myogenic differentiation protocol, compared to previously reported methods.

Recently, it was revealed that premyogenic mesodermal genes are activated by transgenic expression of *MYOD1* in undifferentiated mouse embryonal carcinoma cells [11]. In our hiPSC differentiation method, exogenous *MYOD1* acts as a dominant regulator of myogenesis, through activation of recognized mature myogenic gene networks, presumably without requiring stepwise mesodermal differentiation as occurs during embryonic development. We confirm that exogenous expression of *MYOD1* in undifferentiated hiPSCs can indeed promote premyogenic mesodermal gene expression. However, our knockdown experiments suggest that premyogenic mesodermal gene expression is dispensable, and that the majority of the undifferentiated hiPSC population can be directly differentiated into mature myocytes. This observation supports our hypothesis that Dox-induced *MYOD1* expression in hiPSCs directly activates the myogenic gene network independent of premyogenic mesodermal genes.

Myocytes induced from hiPSCs with *MYOD1* demonstrate similar global gene expression patterns and microstructures to the immortal human myoblast cell line Hu5/E18. Moreover, induced myocytes acquire mature functional properties such as cell fusion and twitching on electrical stimulation. This report is the first to present such detailed analysis for the functional properties of induced myocytes, which will be absolutely critical in attaining reliable muscular disease modeling. We applied our system to rproduce pathological conditions of MM by using patient-derived hiPSCs. We observed defective membrane repair in MM hiPSC-derived myotubes after two-photon laser-induced injury of the sarcolemma, and rescued this phenotype by transgenic expression of full-length *DYSF*. It is still unclear why defective membrane repair may result in chronic muscle inflammation in MM patients. Importantly, DYSFERLIN is also expressed in immune cells [41], and there is some debate as to which cell lineage (myocytes or immune cells) is responsible for the pathology of MM. As immune cells may be differentiated directly from iPSCs [42], this question may be addressed by co-culture of healthy iPSC-derived immune cells and MM patient iPSC-derived myocytes, or vice versa. In this context, our differentiation system should prove useful in deriving enriched myocyte populations for co-culture, and help to resolve the remaining questions regarding MM pathology.

Myogenic differentiation of hiPSCs provides clear advantages over the use of disease myocytes or fibroblasts in recreating pathological conditions, and the *in vitro* study of myogenic disorders. Our defined differentiation system provides reproducibility, high efficiency and short induction periods. These properties could help promote the establishment of human muscular disease models, which would eventually lead to a better understanding of disease development. Furthermore, drug-screening platforms based on human cells will help resolve incongruent drug treatment efficacies observed between mice and human, hopefully leading to prospective treatments and eventually cures.

Methods

Cell Culture

Human iPSC lines 201B7, 253G1 and 253G4 were kindly provided by Dr. Shinya Yamanaka [1]. Human dermal fibroblasts used for generating 201B7 and 253G4 were purchased from Cell Applications, Inc. All human iPS cells were established according to procedures approved by the Ethics Committee on Human Stem Cell Research of the Institute for Frontier Medical Sciences, Kyoto University. The ethics committee approved our studies. The hiPSCs were cultured in human iPS medium composed of primate ES medium (ReproCELL) supplemented with 4 ng/mL recombinant human basic fibroblast growth factor (bFGF, Wako), and otherwise maintained as previously described [1]. The immortalized human myoblast cell line Hu5/E18 provided by RIKEN BRC through the National Bio-Resource Project of the MEXT, Japan, was maintained and differentiated as described previously [32].

Generation of an iPS Cell Line Derived from a Patient with Miyoshi Myopathy (MM)

Studies were approved by the authors' Institutional Review Board and conducted under the Declaration of Helsinki. MM patient information was encoded to protect privacy, and written informed consent obtained. The MM patient was known to have 2 mutations in the *DYSF* gene. Fibroblasts from the patient were cultured from skin biopsy explants under protocols approved by the Ethics Committee on Human Stem Cell Research of the Graduate School of Medical Sciences, Kumamoto University. The ethics committee specifically approved these studies. The patient provided written informed consent to participate in these studies. Skin samples were minced and cultured in Dulbecco's Modified Eagle's Medium (DMEM; Invitrogen) supplemented with 10% fetal bovine serum (Invitrogen). Patient-derived hiPSCs were generated with SeV as described previously [43] and are referred to herein as MM-hiPSCs.

Generation of a Doxycycline-inducible MyoD-hiPS Cell Line

A cDNA clone of *MYOD1* was purchased from MGC clone (Invitrogen, MGC:71135, GenBank: BC064493.1). The coding region of *MYOD1* was PCR cloned into pENTR Directional TOPO (Invitrogen) according to the manufacturer's protocol. The PB-TAC-ERN (KW111) vector was assembled with standard cloning methods by using PB-TET [19] as a backbone. The βgeo reporter in PB-TET was swapped for mCherry, and a constitutive rtTA-neo expression cassette inserted. pVITRO1-neo (InvivoGen) was introduced at the 3′ end of the construct. Details of the cloning steps are available upon request. Using Gateway cloning, the *MYOD1* cDNA was transferred to the PB-TAC-ERN destination vector as indicated in **Fig. 1a**, to yield the transposon PB-MyoD1.

Plasmid DNA for transfection was prepared using a QIAprep Spin Miniprep Kit (Qiagen). Non-diseased control hiPSCs and MM-hiPSCs were seeded onto mitomycin C-treated SNL feeder cells [1] in a 6-well culture dish. The next day, 1 μg destination vector and 1 μg PBase plasmid [19] were transfected into hiPSCs with FuGENE HD (Roche), according to the manufacturer's protocol. Forty-eight hours after transfection, 100 μg/mL G418 (Nacalai Tesque) was added to select for stable Tet-MyoD1 transposition, clones were picked, and the appropriate MyoD-hiPSC clones with high mCherry expression selected.

Overexpression of *DYSFERLIN* in MM Patient-derived iPSCs

Full-length *DYSF* cDNA was kindly provided by the Jain Foundation. The *DYSF* cDNA was Gateway cloned into a PB-based, EF1α promoter-driven constitutive expression vector which co-expresses puromycin resistance (PB-Dysferlin). MyoD-MM-

hiPSCs were seeded onto mitomycinC-treated SNL-PH feeder cells (resistant to neomycin, puromycin, and hygromycin). The next day, 1 μg of both PB-Dysferlin and PBase [19] plasmids were transfected into MyoD-MM-hiPSCs by using FuGENE HD (Roche), as described above. Forty-eight hours after transfection, 100 μg/mL G418 (Nacalai Tesque) and 1 μg/mL Puromycin (Nacalai Tesque) were added to select for cells carrying both the Tet-MyoD and PB-Dysferlin vectors. After selection, MyoD-MM+Dysferlin hiPSC clones displaying DYSFERLIN expression were selected by western Blotting.

Differentiation of MyoD-hiPSCs

MyoD-hiPSCs were seeded onto CollagenI (Iwaki) or Matrigel (BD Biosciences) coated dishes without feeder cells. Matrigel was diluted 1:50 with primate ES medium. MyoD-hiPSCs were trypsinized and dissociated into single cells. The cell number plated ranged from 2.0×10^5 to 1.0×10^6 per $10cm^2$. Culture medium was changed to human iPS medium without bFGF and with 10 μM Y-27632 (Nacalai Tesque). After 24 h, 1 μg/mL doxycycline (LKT Laboratories) was added to the culture medium. After an additional 24 h, culture medium was changed to differentiation medium composed of alpha Minimal Essential Medium (αMEM; Nacalai Tesque) with 5% KSR (Invitrogen), 50 mU/L Penicillin/50 μg/L Streptomycin (Invitrogen), and 100 μM 2-Mercaptoethanol (2-ME). After an additional 5 days, culture medium was changed to DMEM with 5% horse serum (Sigma), 50 mU/L Penicillin/50 μg/L Streptomycin, 10 ng/mL recombinant human insulin-like growth factor 1 (Peprotech), 2 mM L-Glutamine and 100 μM 2-ME. Approximately 2 days later, myogenic properties were assessed.

Fluorescence Activated Cell Sorting Analysis of mCherry Positive Cells

Doxycycline-treated cells were washed in Phosphate buffered saline (PBS) and incubated for 5 min with 0.25% Trypsin to dissociate into single cells. After cells were counted, they were suspended in Hank's balanced salt solution (Life technologies), supplemented with 1% BSA at 1.0×10^6 cells/100 μL and analyzed on an LSR Fortessa (BD Biosciences) for the expression of mCherry.

RNA Isolation and Reverse Transcription

Total RNA was isolated using Sepazol (Nacalai Tesque) according to the manufacturer's protocol. Residual genomic DNA was digested and removed using DNase I (Invitrogen) treatment. First strand cDNA was synthesized using the Superscript III First-Strand Synthesis System (Invitrogen) and random hexamer primers or oligo (dT) according to experimental aims. Reverse transcription and conventional PCR were performed as described previously [1]. Quantitative PCR was performed using probe sets, SYBR Green (Applied Biosystems), and Step One thermal cycler (Applied Biosystems). β-actin was used as an internal controls. For standardization, we set the value of the d0, d5 or d7 sample as the control value (= 1.0). Primers used in this study are listed in **Table S1**.

Transplantation Studies

All mouse experiments were carried out according to protocols approved by the Animal Research Committee of Kyoto University. The committee specifically approved these animal studies. NOD/Scid mice were purchased from Charles River Laboratories, and were mated with DMD-null mice (which do not express DYSTROPHIN) to generate the NOD/Scid-DMD mice used for *in vivo* transplantation studies. Mice were anesthetized with diethyl ether and injured with cardiotoxin before intramuscular cell transplantation. Twenty-four hours after cardiotoxin damage, d6 Dox-treated MyoD-hiPSCs (1.0×10^6–9.5×10^6 cells per 50 mL 10% Matrigel in αMEM) were injected into left TA muscles. All mice used in this study were humanely sacrificed 28 days after transplantation and tissue samples were collected. Collected samples were embedded into a pedestal of tragacanth gum.

Engrafted muscles were frozen in isopentane cooled in liquid nitrogen. Serial cryosections (10–20 μm) were collected. Tissue cryosections were fixed and stained as described previously [44]. Briefly, tissue cryosections were fixed using 4% paraformaldehyde (PFA)/PBS for 20 min. Samples were blocked with 1% Goat serum (Sigma), 0.1% Bovine serum Albumin (Sigma), 0.2% Triton X-100 (Nacalai Tesque)/PBS for 60 min. Samples were incubated with primary antibodies for 16–18 h at 4°C. Next day, samples were washed 3 times in PBS and incubated with secondary antibodies for 1 h at room temperature. 4,6-Diamidino-2-phenylindole (DAPI; 1:5000) was used to counter-stain nuclei. PermaFluor (Thermo Scientific) was used as a mounting agent. Samples were observed by LMS710 confocal microscopy (Carl Zeiss).

Teratoma Formation Assay

For teratoma formation, sub-confluent undifferentiated human iPSCs were harvested and resuspended in maintenance medium containing 50% Matrigel. Human iPSCs were injected into tibialis anterior muscles of NOD/scid mice by using pre-chilled syringe with a 27G needle. Mice were sacrificed for assays 4 weeks after transplantation.

Co-culture with C2C12 Cells

Differentiated MyoD-hiPSCs were co-cultured with a C2C12 cell line which expresses GFP constitutively from the CAG promoter (kindly provided Dr. Kurisaki, Department of Growth Regulation, Institute for Frontier Medical Sciences, Kyoto University). MyoD-hiPSCs were differentiated for 7 days according our protocol. On d7, medium was replaced with DMEM supplemented with 5% horse serum, and 1.0×10^5 C2C12 cells were seeded onto MyoD-hiPSCs. Bio Station CT (Nikon) was used for time-lapse observation of co-cultured samples. The duration of image acquisition was 1 h.

Immunohistochemistry of Cultured Cells

Cells were fixed and stained as described previously [1]. Briefly, cells were fixed using 2% PFA/PBS. Samples were blocked with 5% Blocking One (Nacalai Tesque)/PBS for 30 min and then incubated with primary antibodies diluted in 5% Blocking One/PBS for 16–18 h at 4°C. Next, samples were washed 3 times in PBS and incubated with secondary antibodies diluted in 5% Blocking One/PBS for 1 h at room temperature. DAPI (1:5000;Sigma) was used to counter-stain nuclei. Antibodies are listed below. For mitochondrial staining, MitoTracker Red CMXRos (Invitrogen) was used according to the manufacturers protocol. Samples were observed with a BZ-9000E (Keyence).

Western Blotting

Cells were harvested and analyzed as described previously [1]. Briefly, semiconfluent cells were lysed in RIPA buffer (50 mM Tris-HCl, pH 8.0, 150 mM NaCl, 1% Nonidet P-40 (NP-40), 1% sodium deoxycholate, and 0.1% SDS), supplemented with protease inhibitor cocktail (Roche). Cell lysates (10 μg) were separated by electrophoresis on 8% or 12% SDS-polyacrylamide gel and

transferred to a polyvinylidine difluoride membrane (Millipore). The blot was blocked with TBST (20 mM Tris-HCl, pH 7.6, 136 mM NaCl, and 0.1% Tween-20) containing 1% skim milk and then incubated with primary antibody solution at 4°C overnight. After washing with TBST, the membrane was incubated with secondary antibody for 1 h at room temperature. Signals were detected with Immobilon Western chemiluminescent HRP substrate (Millipore) and ChemiDoc XRS+imaging system (BIO-RAD). Antibodies are listed below.

Primary and Secondary Antibodies

Primary antibodies used in this study were as follows: rat, anti-Laminin monoclonal antibody (mAb; 1:15; Alexis), mouse Anti-human Myosin heavy chain mAb (MF20; 1:400; R&D), mouse anti-myogenin mAb (F5D; 1:400; Santa Cruz), rabbit anti-MyoD polyclonal antibody (pAb; M-318, 1:400; Santa Cruz), mouse anti-human Spectrin mAb (1:100; Leica), mouse anti-human nuclei mAb (1:200; Millipore), mouse anti-alpha skeletal muscle actin mAb (1:200; Acris), rabbit anti-Creatine Kinase M pAb (Y14; 1:100; Bioworld Technology), mouse anti-Dysferlin mAb (NCL-Hamlet, 1:25; Leica), mouse anti-Dystrophin mAb (NCL DYS1, 1:100; Leica), mouse anti-SSEA-4 mAb (1:100; Millipore), mouse anti-TRA-1-81 mAb (1:100; Millipore), and mouse anti-Nanog mAb (1E6C4, 1:2000; Cell Signaling).

Secondary antibodies used in this study were as follows: Alexa Fluor 488 conjugated goat-anti-rabbit or mouse IgG, Alexa Fluor 568 conjugated goat-anti- rabbit or mouse IgG (1:500; Invitrogen), and HRP conjugated goat-anti-mouse IgG (1:200 for IHC, 1:2000 for western blotting; Vector).

Statistical Analysis

Differences between samples were assessed by using the Student's two-tailed *t* test for independent samples.

Electron Microscopy

Samples were chemically fixed and observed by Tokai Electron Microscopy, Inc. according to their protocol (Tokai Electron Microscopy, Inc.). Briefly, Samples were fixed with 2% PFA/PBS, 2% glutaraldehyde (GA) in 0.1 M phosphate buffer (Pb), pH 7.4 at 37°C and put them into a refrigerator (4°C) for 30 min. Thereafter, they were fixed with 2% GA in 0.1 M Pb at 4°C overnight. After these fixation the samples were rinsed 3 times with 0.1 M Pb for 30 min each, followed by post fixation with 2% osmium tetroxide (OsO4) in 0.1 M Pb at 4°C for 1 h.

The samples were dehydrated through a series of graded ethanol (50%, 70%, 90%, and 100%). The schedule was as follows: 50% and 70% for 5 min each at 4°C, 90% for 5 min at room temperature, and 3 changes of 100% for 5 min each at room temperature.

The samples were transferred to a resin (Quetol-812; Nisshin EM Co., Tokyo, Japan), and polymerized at 60°C for 48 h.

The blocks were ultra-thin sectioned at 70 nm with a diamond knife using a ultramicrotome (ULTRACUT UCT; Leica) and sections were placed on copper grids. They were stained with 2% uranyl acetate at room temperature for 15 min, and then rinsed with distilled water followed by being secondary-stained with Lead stain solution (Sigma-Aldrich Co.,) at room temperature for 3 min.

The grids were observed by a transmission electron microscope (JEM-1200EX; JEOL Ltd.,) at an acceleration voltage of 80 kV. Digital images (2048×2048 pixels) were taken with a CCD camera (VELETA; Olympus Soft Imaging Solutions GmbH).

Microarray

Total RNA from each condition was obtained from samples by using the RNeasy Mini Kit (Qiagen) according to the manufacturer's instructions. The quality of RNA samples were determined to be sufficient for Microarray analysis by using the Agilent RNA 6000 Nano Assay (Agilent Technologies). After confirming the quality of RNA, cRNA was synthesized on day one. On d2, cDNA was synthesized and purified. *In vitro* transcription and biotin labeling, and hybridization to the GeneChip ST Array (Affymetrix) were performed according to Affymetrix protocols on d3 and 4. Samples were loaded onto a Fluidics station (Affymetrix) and their signals were analyzed.

Microarray Data Analysis

Affymetrix CEL files were imported into GeneSpringGX 11.5.1. Probe intensities were normalized, and expression signals of all genes (probe sets) were calculated using RMA 16 as implemented in GeneSpring software. The data were grouped into those of undifferentiated hiPSCs, MyoD-hiPSCs derived myocytes, and Hu5/E18 derived myocytes. Upregulated genes were identified by at least 2-fold changes. A heat map was created using a clustering function algorithm of on both entities and conditions. Distance metric was Euclidean. Linkage rule was single. Myogenic upregulated genes were assembled arbitrarily. As statistical analysis, multiscale bootstrap clustering was performed.

siRNA Transfection

The siRNAs targeting T, TBX6 and a scrambled negative control were purchased (Sigma, SASI_Hs01_00221962, SASI_Hs01_00166068 and SIC-001-10). siRNA (50 nM) was transfected into hiPSCs seeded at a density of 2.0 to 3.0×10^5 cells per $10cm^2$ on d0 and d3, respectively, using Lipofectamine RNAiMAX (Invitrogen) according to the manufacturer's protocol.

Membrane Repair Assay

Membrane repair assays were performed using differentiated myotubes as described previously [17]. Briefly, membrane damage was induced in the presence of FM1-43 dye (2.5 mM; MolecularProbes) with a two-photon confocal laser-scanning microscope (LSM710NLO; Zeiss) coupled to a 10-W Argon/Ti:sapphire laser. Images were captured beginning 20 s before (t = 0) and for 3 min after irradiation at 10 s intervals. For every image taken, the fluorescence intensity at the site of damage was measured with Zeiss LSM 710NLO imaging software.

Electrical Stimulation

Electrical stimulation was performed using differentiated MyoD-hiPSCs at around d14 by using C-Dish (ION Optics) as previously described [45]. We loaded electrical voltage with the electric stimulator (Uchida Denshi) at 100 V onto differentiated myotubes for 3 msec at repeated 1 s intervals.

Supporting Information

Figure S1 Evaluation of pluripotency of MyoD-hiPSCs. (**a**) Immunohistochemistry of undifferentiated markers. Scale bar = 100 μm. (**b**) RT-PCR analysis for undifferentiated markers. (**c**) Teratoma formation assay from MyoD-hiPSCs and empty vector transduced hiPSCs. H&E staining of teratoma formed in TA muscle from NOD/scid mouse. Three germ layers formed in teratoma were shown in each panel, respectively. Arrows indicate each germ layer, respectively. Scale bars = 100 μm.
(TIF)

Figure S2 Evaluation for MyoD-hiPSC clones. (**a**) Expression of mCherry which is synonymous with exogenous *MyoD1* driven by Dox treatment for 24 h. (**b**) RT-PCR analyses of MyoD-hiPSC clones. Cloned MyoD-hiPSCs had no leaky expression of exogenous *MyoD1* without Dox, while they could express exogenous *MyoD1* 24 h after Dox addition. Endogenous *MYOD1* could be promoted 96 h after Dox addition.
(TIF)

Figure S3 Other myogenic induction methods by SB-OGs system or changing Dox-addition days. (**a**) Protocol of myogenic induction via EB outgrowth. (**b**) Expression of mCherry and immunohistochemistry of MHC. Scale bars = 100 μm. (**c**) Protocol of changing the timing of dox-addition. (**d**) The percentage of MHC positive cells per total cells. $^{**}p<0.01$.
(TIF)

Figure S4 Expression of premyogenic mesodermal markers. Quantitative real time PCR for premyogenic markers was performed during MyoD-hiPSC differentiation in B7 #9 MyoD-hiPSC clone with (gray bars) or without (black bars) Dox administration (n = 3). Data are shown as the mean ± SD. The data were standardized by β-actin using embryoid body. The data on d5 or d7 = 1. $^{*}p<0.05$, $^{**}p<0.01$, respectively.
(TIF)

Figure S5 Suppression of mesodermal markers by siRNA. The siRNA reagent targeting T or TBX6 was added to differentiation culture of MyoD-hiPSCs (clone B7 #9) at d0 or d3 (**a, b**). Quantitative real time PCR was then performed on d3 (**a**) or d5 (**b**) (n = 3). The expression of PAX3 was suppressed by siRNAs for both T and TBX6. $^{*}p<0.05$ (**c**) The expression of MHC in differentiated MyoD-hiPSCs with or without siRNA treatment on d9. Scale bar = 100 μm. (**d**) Percentage of MHC positive cells 9 days after differentiation with or without siRNA treatment in B7 #9 MyoD-hiPSC clone (n = 3).
(TIF)

Figure S6 Multiscale bootstrap clustering for the data from microarray. The number of repeated calculation was 1000 times. Abbreviated words "AU" and "BP" means "approximately unbiased p-value" and "bootstrap probability," respectively. Distance means correlation. Cluster method was average.
(TIF)

Figure S7 Confirmation of the data obtained from microarray by quantitative real time PCR. (**a**) Relative gene expression of transcription factors which are significant in microarray analyses. Data are listed as mean ± S.D. The data were standardized by β-actin using teratoma. The data on d0 = 1. The data in *Endo-MYOD1, MYOGENIN, MEF2C* and *SIX1* were expressed with logarithmic Y axes because differentiated cells showed extremely high values, respectively. $^{**}p<0.01$.
(TIF)

Figure S8 Fusion potential *in vivo*. Immunohistochemistry of TA muscles from NOD/Scid-DMD mice after 28 days after transplantation of d6 MyoD-hiPSCs. Scale bars = 20 μm. (**a**) Human Spectrin expression (red) was detected along with Laminin (green). (**b**) Human DYSTROPHIN expression (green) was detected along with Laminin (white).
(TIF)

Figure S9 Teratoma formation assay from MyoD-MM hiPSCs. (**a**) H&E staining of teratoma formed in TA muscle from NOD/scid mouse. Scale bar = 100 μm. (**b**) H&E staining of three germ layers formed in teratoma. Arrows indicate each germ layer, respectively. Scale bars = 100 μm.
(TIF)

Table S1 PCR-primers were listed for both RT-PCR and quantitative real-time RT-PCR.
(DOCX)

Movie S1 The MyoD-hiPSCs changed their shape to spindle-like uniformly during differentiation from d1 to d7.
(WMV)

Movie S2 Contraction of myofiber derived from MyoD-hiPSCs at differentiation d14 by electric stimulation.
(WMV)

Movie S3 Fusion of hiPS cells with murine myofiber. Red shows human and green shows murine derived myogenic cells.
(WMV)

Movie S4 Membrane repair assay of MyoD-hiPSC derived myofibers from MM patient. Red circle indicates damaged point.
(WMV)

Movie S5 Membrane repair assay of MyoD-hiPSC derived myofibers from MM patient with DYSFERLIN over-expression. Red circle indicates damaged point.
(WMV)

Movie S6 Membrane repair assay of MyoD-hiPSC derived myofibers from non-disease control. Red circle indicates damaged point.
(WMV)

Acknowledgments

We would like to thank I. Maki for technical assistance. We also thank Dr. T. Sato and Dr. A. Watanabe for valuable scientific discussion, and Dr. S. Yamanaka and Dr. T. Kurisaki for providing human iPS cells and the GFP-expressing C2C12 cell line, respectively. The cDNA for human *DYSF* was kindly provided by the Jain Foundation.

Author Contributions

Conceived and designed the experiments: AT KW KM MI AS KI EK HS. Performed the experiments: AT KW KM TN ES EK. Analyzed the data: AT KW TY KM HS. Contributed reagents/materials/analysis tools: AT KW AH YM NF KH TE SY. Wrote the paper: AT KW HS.

References

1. Takahashi K, Tanabe K, Ohnuki M, Narita M, Ichisaka T, et al. (2007) Induction of pluripotent stem cells from adult human fibroblasts by defined factors. Cell 131: 861–872.
2. Yu J, Vodyanik MA, Smuga-Otto K, Antosiewicz-Bourget J, Frane JL, et al. (2007) Induced pluripotent stem cell lines derived from human somatic cells. Science 318: 1917–1920.
3. Tiscornia G, Vivas EL, Belmonte JC (2011) Diseases in a dish: modeling human genetic disorders using induced pluripotent cells. Nature medicine 17: 1570–1576.
4. Barberi T, Bradbury M, Dincer Z, Panagiotakos G, Socci ND, et al. (2007) Derivation of engraftable skeletal myoblasts from human embryonic stem cells. Nature medicine 13: 642–648.
5. Mahmood A, Harkness L, Schroder HD, Abdallah BM, Kassem M (2010) Enhanced differentiation of human embryonic stem cells to mesenchymal progenitors by inhibition of TGF-beta/activin/nodal signaling using SB-431542. Journal of bone and mineral research : the official journal of the American Society for Bone and Mineral Research 25: 1216–1233.

6. Darabi R, Arpke RW, Irion S, Dimos JT, Grskovic M, et al. (2012) Human ES- and iPS-derived myogenic progenitors restore DYSTROPHIN and improve contractility upon transplantation in dystrophic mice. Cell stem cell 10: 610–619.
7. Osafune K, Caron L, Borowiak M, Martinez RJ, Fitz-Gerald CS, et al. (2008) Marked differences in differentiation propensity among human embryonic stem cell lines. Nature biotechnology 26: 313–315.
8. Davis RL, Weintraub H, Lassar AB (1987) Expression of a single transfected cDNA converts fibroblasts to myoblasts. Cell 51: 987–1000.
9. Mizuno H, Zuk PA, Zhu M, Lorenz HP, Benhaim P, et al. (2002) Myogenic differentiation by human processed lipoaspirate cells. Plastic and reconstructive surgery 109: 199–209; discussion 210–191.
10. Tapscott SJ, Davis RL, Thayer MJ, Cheng PF, Weintraub H, et al. (1988) MyoD1: a nuclear phosphoprotein requiring a Myc homology region to convert fibroblasts to myoblasts. Science 242: 405–411.
11. Gianakopoulos PJ, Mehta V, Voronova A, Cao Y, Yao Z, et al. (2011) MyoD directly up-regulates premyogenic mesoderm factors during induction of skeletal myogenesis in stem cells. The Journal of biological chemistry 286: 2517–2525.
12. Warren L, Manos PD, Ahfeldt T, Loh YH, Li H, et al. (2010) Highly efficient reprogramming to pluripotency and directed differentiation of human cells with synthetic modified mRNA. Cell stem cell 7: 618–630.
13. Tedesco FS, Gerli MF, Perani L, Benedetti S, Ungaro F, et al. (2012) Transplantation of genetically corrected human iPSC-derived progenitors in mice with limb-girdle muscular dystrophy. Science translational medicine 4: 140ra189.
14. Goudenege S, Lebel C, Huot NB, Dufour C, Fujii I, et al. (2012) Myoblasts Derived From Normal hESCs and Dystrophic hiPSCs Efficiently Fuse With Existing Muscle Fibers Following Transplantation. Molecular therapy : the journal of the American Society of Gene Therapy.
15. Ozasa S, Kimura S, Ito K, Ueno H, Ikezawa M, et al. (2007) Efficient conversion of ES cells into myogenic lineage using the gene-inducible system. Biochemical and biophysical research communications 357: 957–963.
16. Miyoshi K, Kawai H, Iwasa M, Kusaka K, Nishino H (1986) Autosomal recessive distal muscular dystrophy as a new type of progressive muscular dystrophy. Seventeen cases in eight families including an autopsied case. Brain : a journal of neurology 109 (Pt 1): 31–54.
17. Bansal D, Miyake K, Vogel SS, Groh S, Chen CC, et al. (2003) Defective membrane repair in dysferlin-deficient muscular dystrophy. Nature 423: 168–172.
18. Liu J, Aoki M, Illa I, Wu C, Fardeau M, et al. (1998) Dysferlin, a novel skeletal muscle gene, is mutated in Miyoshi myopathy and limb girdle muscular dystrophy. Nature genetics 20: 31–36.
19. Woltjen K, Michael IP, Mohseni P, Desai R, Mileikovsky M, et al. (2009) piggyBac transposition reprograms fibroblasts to induced pluripotent stem cells. Nature 458: 766–770.
20. Sarkar S, Cooke PH (1970) In vitro synthesis of light and heavy polypeptide chains of myosin. Biochemical and biophysical research communications 41: 918–925.
21. Blau HM, Pavlath GK, Hardeman EC, Chiu CP, Silberstein L, et al. (1985) Plasticity of the differentiated state. Science 230: 758–766.
22. Adewumi O, Aflatoonian B, Ahrlund-Richter L, Amit M, Andrews PW, et al. (2007) Characterization of human embryonic stem cell lines by the International Stem Cell Initiative. Nat Biotechnol 25: 803–816.
23. Wright WE, Sassoon DA, Lin VK (1989) Myogenin, a factor regulating myogenesis, has a domain homologous to MyoD. Cell 56: 607–617.
24. Nigro JM, Schweinfest CW, Rajkovic A, Pavlovic J, Jamal S, et al. (1987) cDNA cloning and mapping of the human creatine kinase M gene to 19q13. American journal of human genetics 40: 115–125.
25. Monaco AP, Neve RL, Colletti-Feener C, Bertelson CJ, Kurnit DM, et al. (1986) Isolation of candidate cDNAs for portions of the Duchenne muscular dystrophy gene. Nature 323: 646–650.
26. Hashimoto K, Fujimoto H, Nakatsuji N (1987) An ECM substratum allows mouse mesodermal cells isolated from the primitive streak to exhibit motility similar to that inside the embryo and reveals a deficiency in the T/T mutant cells. Development 100: 587–598.
27. Saga Y, Hata N, Koseki H, Taketo MM (1997) Mesp2: a novel mouse gene expressed in the presegmented mesoderm and essential for segmentation initiation. Genes & development 11: 1827–1839.
28. Chapman DL, Agulnik I, Hancock S, Silver LM, Papaioannou VE (1996) Tbx6, a mouse T-Box gene implicated in paraxial mesoderm formation at gastrulation. Developmental biology 180: 534–542.
29. Goulding MD, Chalepakis G, Deutsch U, Erselius JR, Gruss P (1991) Pax-3, a novel murine DNA binding protein expressed during early neurogenesis. The EMBO journal 10: 1135–1147.
30. Tajbakhsh S, Rocancourt D, Cossu G, Buckingham M (1997) Redefining the genetic hierarchies controlling skeletal myogenesis: Pax-3 and Myf-5 act upstream of MyoD. Cell 89: 127–138.
31. Hashimoto N, Kiyono T, Wada MR, Shimizu S, Yasumoto S, et al. (2006) Immortalization of human myogenic progenitor cell clone retaining multipotentiality. Biochemical and biophysical research communications 348: 1383–1388.
32. Hashimoto N, Kiyono T, Wada MR, Umeda R, Goto Y, et al. (2008) Osteogenic properties of human myogenic progenitor cells. Mechanisms of development 125: 257–269.
33. Ott MO, Bober E, Lyons G, Arnold H, Buckingham M (1991) Early expression of the myogenic regulatory gene, myf-5, in precursor cells of skeletal muscle in the mouse embryo. Development 111: 1097–1107.
34. Dodou E, Xu SM, Black BL (2003) mef2c is activated directly by myogenic basic helix-loop-helix proteins during skeletal muscle development in vivo. Mechanisms of development 120: 1021–1032.
35. Ishibashi J, Perry RL, Asakura A, Rudnicki MA (2005) MyoD induces myogenic differentiation through cooperation of its NH2- and COOH-terminal regions. The Journal of cell biology 171: 471–482.
36. Kudoh H, Ikeda H, Kakitani M, Ueda A, Hayasaka M, et al. (2005) A new model mouse for Duchenne muscular dystrophy produced by 2.4 Mb deletion of dystrophin gene using Cre-loxP recombination system. Biochemical and biophysical research communications 328: 507–516.
37. Bittner RE, Anderson LV, Burkhardt E, Bashir R, Vafiadaki E, et al. (1999) Dysferlin deletion in SJL mice (SJL-Dysf) defines a natural model for limb girdle muscular dystrophy 2B. Nature genetics 23: 141–142.
38. Sicinski P, Geng Y, Ryder-Cook AS, Barnard EA, Darlison MG, et al. (1989) The molecular basis of muscular dystrophy in the mdx mouse: a point mutation. Science 244: 1578–1580.
39. Kunkel LM, Bachrach E, Bennett RR, Guyon J, Steffen L (2006) Diagnosis and cell-based therapy for Duchenne muscular dystrophy in humans, mice, and zebrafish. Journal of human genetics 51: 397–406.
40. Tiscornia G, Vivas EL, Izpisua Belmonte JC (2011) Diseases in a dish: modeling human genetic disorders using induced pluripotent cells. Nature medicine 17: 1570–1576.
41. Nagaraju K, Rawat R, Veszelovszky E, Thapliyal R, Kesari A, et al. (2008) Dysferlin deficiency enhances monocyte phagocytosis: a model for the inflammatory onset of limb-girdle muscular dystrophy 2B. The American journal of pathology 172: 774–785.
42. Niwa A, Heike T, Umeda K, Oshima K, Kato I, et al. (2011) A novel serum-free monolayer culture for orderly hematopoietic differentiation of human pluripotent cells via mesodermal progenitors. PloS one 6: e22261.
43. Fusaki N, Ban H, Nishiyama A, Saeki K, Hasegawa M (2009) Efficient induction of transgene-free human pluripotent stem cells using a vector based on Sendai virus, an RNA virus that does not integrate into the host genome. Proc Jpn Acad Ser B Phys Biol Sci 85: 348–362.
44. Sakurai H, Okawa Y, Inami Y, Nishio N, Isobe K (2008) Paraxial mesodermal progenitors derived from mouse embryonic stem cells contribute to muscle regeneration via differentiation into muscle satellite cells. Stem Cells 26: 1865–1873.
45. Manabe Y, Miyatake S, Takagi M, Nakamura M, Okeda A, et al. (2012) Characterization of an Acute Muscle Contraction Model Using Cultured C2C12 Myotubes. PloS one 7: e52592.

nature chemical biology

ARTICLE

PUBLISHED ONLINE: 15 DECEMBER 2013 | DOI: 10.1038/NCHEMBIO.1410

VMAT2 identified as a regulator of late-stage β-cell differentiation

Daisuke Sakano[1], Nobuaki Shiraki[1], Kazuhide Kikawa[1,2], Taiji Yamazoe[1], Masateru Kataoka[1], Kahoko Umeda[1], Kimi Araki[3], Di Mao[4], Shirou Matsumoto[2], Naomi Nakagata[5], Olov Andersson[6,7], Didier Stainier[6,8], Fumio Endo[2], Kazuhiko Kume[1,10], Motonari Uesugi[4] & Shoen Kume[1,9]*

Cell replacement therapy for diabetes mellitus requires cost-effective generation of high-quality, insulin-producing, pancreatic β cells from pluripotent stem cells. Development of this technique has been hampered by a lack of knowledge of the molecular mechanisms underlying β-cell differentiation. The present study identified reserpine and tetrabenazine (TBZ), both vesicular monoamine transporter 2 (VMAT2) inhibitors, as promoters of late-stage differentiation of *Pdx1*-positive pancreatic progenitor cells into *Neurog3* (referred to henceforth as *Ngn3*)-positive endocrine precursors. VMAT2-controlled monoamines, such as dopamine, histamine and serotonin, negatively regulated β-cell differentiation. Reserpine or TBZ acted additively with dibutyryl adenosine 3′,5′-cyclic AMP, a cell-permeable cAMP analog, to potentiate differentiation of embryonic stem (ES) cells into β cells that exhibited glucose-stimulated insulin secretion. When ES cell-derived β cells were transplanted into AKITA diabetic mice, the cells reversed hyperglycemia. Our protocol provides a basis for the understanding of β-cell differentiation and its application to a cost-effective production of functional β cells for cell therapy.

Pancreatic cells arise from definitive endoderm and Pdx1-positive (Pdx1+) pancreatic progenitor cells[1], which proliferate and give rise to all three pancreatic lineages: acini, ducts and endocrine islets[2]. Endocrine precursors are characterized by the transient expression of the basic helix-loop-helix transcription factor neurogenin 3 (Ngn3, also known as Neurog3)[2]. Previous studies showed that Ngn3 specifically establishes the endocrine lineages and that loss of Ngn3 precludes endocrine cell development[2,3]. Production of islet cells occurs through the concerted activation of a combination of transcription factors[4]. However, the coordination of cell fate decisions remains poorly understood.

The prevalence of diabetes mellitus in many populations is high, and development of cell replacement therapy through generation of β cells from ES cells is a research priority. Recent studies have shown that mouse or human ES cells can be induced to recapitulate embryonic development of the pancreas[5]. Studies on ES cell differentiation into endodermal or pancreatic cell lineages have shown that stimulation with activin, FGF or retinoic acid, in addition to inhibition of hedgehog signaling by KAAD-cyclopamine, promotes the differentiation into endoderm or pancreatic fates[6,7]. New signal pathways that promote ES cell differentiation into endodermal[8] or pancreatic[9] lineages have been discovered through large-scale screening of cell-permeable, bioactive small molecules. However, it is still difficult to derive mature β cells that secrete insulin in a glucose-dependent manner. A better understanding is needed of the underlying molecular mechanisms that control the late stages of β-cell development, in which Pdx1+ pancreatic progenitor cells develop into Ngn3+ endocrine progenitor cells and insulin-positive (Ins+) β cells and then further differentiate into mature β cells capable of glucose-stimulated insulin secretion (GSIS).

Here, we identified reserpine and TBZ as potent promoters of pancreatic progenitor cell differentiation into functional β cells. This study highlights the use of chemical compound libraries for the identification of new developmental pathways that control progenitor cell differentiation into mature β cells.

RESULTS

Reserpine and TBZ increase Ins+ cells

The present study used large-scale screening of chemical compounds with an ES cell line, SK7, that expresses GFP under the *Pdx1* promoter[10,11]. The *Pdx1*-GFP ES cell line is useful because the expression of *Pdx1* is biphasic (**Fig. 1a**), which enabled the detection of early-stage Pdx1+ pancreatic progenitors and late-stage Pdx1+ Ins+ β cells . We optimized the culture to promote modest basal differentiation with high reproducibility, so that the markers *Sox17*, *Pdx1*, *Ngn3* and *Ins1* were sequentially expressed (**Fig. 1a**).

To screen for compounds that potentiate the differentiation of ES cell–derived Pdx1+ pancreatic progenitor cells into insulin-expressing cells, we tested a library of 1,120 biologically active compounds arrayed as single compounds in DMSO on cultures, starting on day 11 after confirming the appearance of *Pdx1*-GFP+ cells and conducting the assay on day 17 (**Fig. 1a**). Candidate compounds that increased both *Ins1* expression and the number of Ins+ cells relative to vehicle (1% DMSO) were selected as primary hits. The coefficient of variation of this screen was 0.36 ± 0.0447 (± s.d.), which was difficult to minimize further owing to the long assay

[1]Department of Stem Cell Biology, Institute of Molecular Embryology and Genetics, Kumamoto University, Kumamoto, Japan. [2]Department of Pediatrics, Graduate School of Medical Sciences, Kumamoto University, Kumamoto, Japan. [3]Laboratory of Developmental Genetics, Institute of Resource Development and Analysis, Kumamoto University, Kumamoto, Japan. [4]Institute for Chemical Research and Institute for Integrated Cell-Material Sciences, (WPI-iCeMS), Kyoto University, Kyoto, Japan. [5]Division of Reproductive Engineering, Center for Animal Resources and Development, Kumamoto University, Kumamoto, Japan. [6]Department of Cell and Molecular Biology, Karolinska Institute, Stockholm, Sweden. [7]Department of Biochemistry and Biophysics, University of California–San Francisco, San Francisco, California, USA. [8]Department of Developmental Genetics, Max Planck Institute for Heart and Lung Research, Bad Nauheim, Germany. [9]Program for Leading Graduate Schools, Health Life Science Interdisciplinary and Global Oriented (HIGO) Program, Kumamoto University, Kumamoto, Japan. [10]Present address: Department of Neuropharmacology, Graduate School of Pharmaceutical Sciences, Nagoya City University, Nagoya, Japan. *e-mail: skume@kumamoto-u.ac.jp

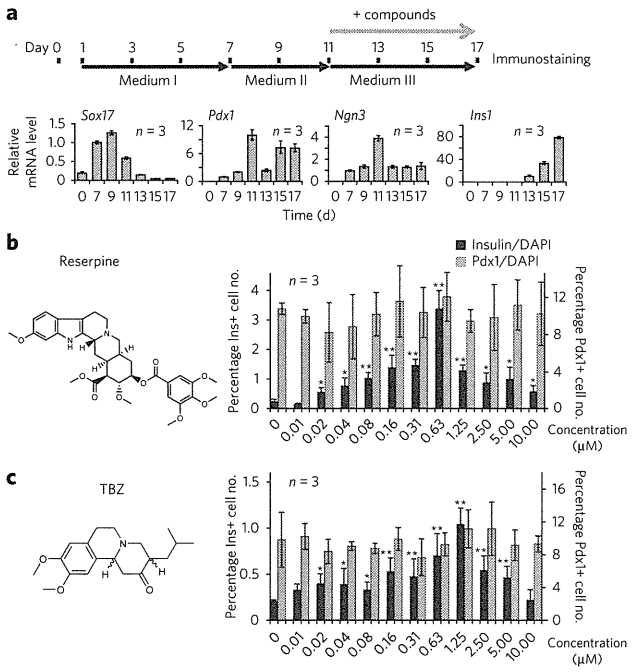

Figure 1 | Reserpine identified as a chemical that enhanced ES cell differentiation into pancreatic β cells. Using a high-throughput screening system, a chemical library was screened, and reserpine was identified as a hit chemical. (**a**) A high-throughput screening system for chemicals that enhance differentiation into β cells. Transcript expressions of *Sox17*, *Pdx1*, *Ngn3* and *Ins1* are expressed as fold change relative to control on day 7. (**b**,**c**) Reserpine (**b**) and TBZ (**c**) (chemical structure shown at left) increased the number of β cells relative to the total number of DAPI-stained cells (black bars) without affecting Pdx1+ cells (light gray bars). In **a**–**c**, data shown are mean ± s.d. ($n = 3$); significant differences between treatment and control at $^*P < 0.05$ and $^{**}P < 0.01$ are shown (two-tailed paired Student's *t*-test).

period. To overcome this, we investigated dose dependencies of the hit chemicals as a secondary screen. Of our hit compounds, the indole alkaloid antipsychotic and antihypertensive drug reserpine demonstrated the strongest effect. Reserpine increased the proportion of Ins+ cells in a concentration-dependent manner without altering the *Pdx1*-GFP+ cell ratio (**Fig. 1b**). Reserpine is known to deplete monoamines from secretory vesicles by blocking uptake into monoamine secretary granules, mediated by VMAT proteins[12–15]. Because human pancreatic β cells express the isoform VMAT2 (refs. 16–19), we also tested another VMAT2 inhibitor, TBZ, which also increased the amount of insulin-expressing cells in a dose-dependent manner (**Fig. 1c**). The half-maximal effective concentration (EC_{50}) values of reserpine and TBZ were 0.19 μM and 0.22 μM, respectively. The concentrations that led to 50% cell death (TD_{50}) were 1.56 μM reserpine and 5.98 μM TBZ. In a separate experiment, we treated cells with 0.63 μM reserpine or 1.25 μM TBZ (**Supplementary Results**, **Supplementary Fig. 1**). We confirmed the increases in the percentage of Ins+ cells out of the total cell numbers versus the untreated cells and in the relative *Ins1* mRNA levels (by real-time PCR) (**Supplementary Fig. 1**). These results suggested that VMAT2 is the candidate target molecule of reserpine and TBZ, which has a pivotal role in the differentiation of ES cells into Ins-expressing cells.

VMAT2 inhibited differentiation into Ins+ cells

To identify the role of VMAT2 in differentiation of ES cells into pancreatic β cells, we performed a knockdown of VMAT2. We established two VMAT2-knockdown SK7 cell lines, VMAT2KD1 and VMAT2KD2, using lentiviral short hairpin RNA (shRNA) (**Fig. 2a**). VMAT2KD2 exhibited lower *Slc18a2* (henceforth referred to as *Vmat2*) expression than VMAT2KD1 (**Fig. 2a**) and showed greater increases in the number of β cells and level of *Ins1* transcription (**Fig. 2b**). These results indicated that reserpine- or TBZ-mediated VMAT2 inhibition led to an enhancement of differentiation into Ins+ cells. Therefore, VMAT2-mediated monoamine storage functions as a negative regulator of differentiation into Ins+ cells. Pancreatic islets have an isozyme of the monoamine-catabolizing enzyme, monoamine oxidase B (MAO_B)[20]. We then tested the effects of application of pargyline, an MAO_B inhibitor (MAO_{Bi}), to stabilize the monoamines and increase intracellular monoamines. Indeed, application of pargyline had an inhibitory effect on the number of β cells and the level of *Ins1* expression, and reserpine counteracted the inhibitory effect of MAO_{Bi} (**Supplementary Fig. 2**). Moreover, the number and expression level of *Pdx1*-GFP+ cells was unaffected (**Supplementary Fig. 2**), similarly to treatment with reserpine and TBZ (**Fig. 1b**,**c**).

Monoamines such as dopamine, histamine and serotonin are known to be the substrates for VMAT2. We tested the effect of these monoamines by exogenous application and found that incubation with dopamine, histamine or serotonin from days 11–17 suppressed β-cell differentiation, with EC_{50} values of 1.25 μM (dopamine), 0.5 μM (histamine) and 0.92 μM (serotonin) (**Fig. 2c–e**). We determined the monoamine contents in the ES cell–derived cells on day 17 (**Fig. 2f–h** and **Supplementary Fig. 3a**,**b**). The dopamine content (approximately 1.3 pg/μg DNA) was approximately 100-fold higher compared to the other monoamines, whereas histamine was undetectable. Inhibition of VMAT2 with TBZ or reserpine and knockdown of *Vmat2* with shRNA significantly decreased ($P < 0.005$) monoamine contents, whereas treatment with pargyline increased it ($P < 0.01$) (**Fig. 2f**,**h** and **Supplementary Fig. 3**). The enzyme that synthesizes dopamine, tyrosine hydroxylase (Th), was expressed in the ES cells during differentiation at a level comparable to that in the embryonic pancreatic bud. By contrast, the histamine-synthesizing enzyme histidine decarboxylase (Hdc) and the serotonin-synthesizing enzyme tryptophan hydroxylase 1 (Tph1) were expressed at approximately 0.066-fold lower levels compared to those in the embryonic pancreas (**Supplementary Fig. 4a–c**). The monoamine receptors dopamine D2 (Drd2), histamine H1 (Hrh1), histamine H2 (Hrh2) and serotonin 1A (Htr1a) were expressed in day 11 and day 13 differentiated cells (**Supplementary Fig. 4d–f**). Upon addition of chemical compounds that inhibit the synthesizing enzymes for dopamine (α-methyl-tyrosine (α-MT) and L-3,4-dihydroxyphenylalanine (L-DOPA)), histamine (α-fluoromethylhistidine (α-FMH)) or serotonin (5-hydroxy tryptophan (5HTP) and carbidopa), we observed increases in Ins+ cell numbers (**Supplementary Fig. 4g–i**).

Taken together, VMAT2-controlled monoamine release exerted inhibitory effects on the differentiation of pancreatic progenitor cells into Ins+ cells. Reserpine and TBZ inhibit the uptake of monoamines into vesicular stores, which led to depletion of monoamines and potentiation of Ins+ cell differentiation.

TBZ increased differentiation into Ngn3+ cells

We then examined the effects of TBZ on marker expression in ES cell–derived cells by real-time PCR. We used TBZ instead of reserpine owing to its lower cytotoxicity; the results are expressed as fold changes compared to control treatments without chemicals at day 13. Treatment with TBZ resulted in a marked increase of *Ngn3*, *Nkx6-1* and *Ins1* transcripts on day 15 and day 17 (**Fig. 3a**). The real-time PCR results suggested that TBZ increases differentiation of ES cell–derived cells into *Ngn3*+ endocrine progenitors. To follow the transient increase of *Ngn3*+ endocrine precursors in living cells, we developed an NGP9 ES cell line from a transgenic mouse line bearing the *Ngn3*-promoter-driven eGFP transgene[21].

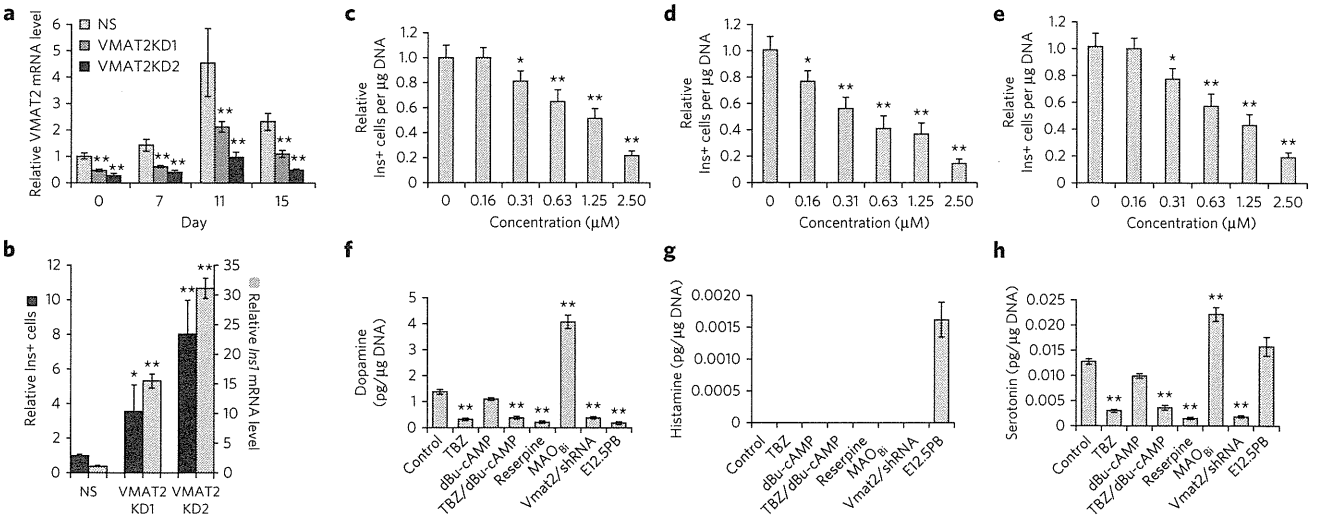

Figure 2 | VMAT2- and monoamine-dependent suppression of pancreatic β-cell differentiation. The effects of VMAT2- and monoamine-mediated inhibition on ES cell differentiation into Ins+ cells were tested, and monoamine cellular contents were determined. (**a**) Time-dependent expression of VMAT2 in VMAT2KD1 (dark gray), VMAT2KD2 (black) and control nonsilencing (NS; light gray) ES cell lines. (**b**) VMAT2KD1 and VMAT2KD2 ES cell lines yielded more Ins+ cells and *Ins1* transcripts than control NS ES cells. (**c**–**e**) Addition of monoamines, dopamine (**c**), histamine (**d**) or serotonin (**e**) suppressed differentiation of ES cells into Ins+ cells in a dose-dependent manner. (**f**–**h**) Cellular contents of dopamine (**f**), histamine (**g**) or serotonin (**h**) when added with VMAT2 inhibitors or MAO_{Bi}, treatment with both TBZ and dBu-cAMP. Control, no chemical treatment; MAO_{Bi}: 1 μM pargyline; Res: 0.63 μM reserpine; MAO_{Bi} + Res: 1 μM pargyline + 0.63 μM reserpine. For **a**–**h**, data shown are mean ± s.d. (n = 3); significant differences between treatment and no chemical treatment at $^*P < 0.05$ and $^{**}P < 0.01$ are shown (two-tailed paired Student's t-test). In **a** and **b**, black bars indicate Ins+ or *Pdx1*-GFP+ relative cell numbers, and gray bars indicate *Ins1* or *Pdx1* transcript expression relative to that in cells with no chemical treatment.

We treated the NGP9 cells with TBZ from day 11 to 13 and then performed the assay on day 13 (**Fig. 3b**). TBZ increased *Ngn3*-GFP+ cell numbers (**Fig. 3b**). These results indicate that VMAT2 signaling negatively controls differentiation into *Ngn3*-GFP+ endocrine precursors. We observed 5-ethynyl-2′-deoxyuridine (EdU) incorporation in Ngn3– cells but not in Ngn3+ cells, and TBZ addition did not increase EdU+ Ngn3+ cells, indicating that the increase in Ngn3+ cells was due to increased differentiation into Ngn3+ cells but not proliferation of Ngn3+ cells (**Fig. 3b** and **Supplementary Fig. 5a**). The Ngn3+ cells expressed Nkx2.2 and Nkx6.1 in their nuclei (**Supplementary Fig. 5b**).

We then examined whether this mechanism existed during normal embryonic development using an *in vitro* pancreas bud culture system. Upon addition of TBZ, we observed increased differentiation into insulin-, glucagon-, somatostatin- or pancreas polypeptide–expressing endocrine cells in the *Pdx1*-GFP+

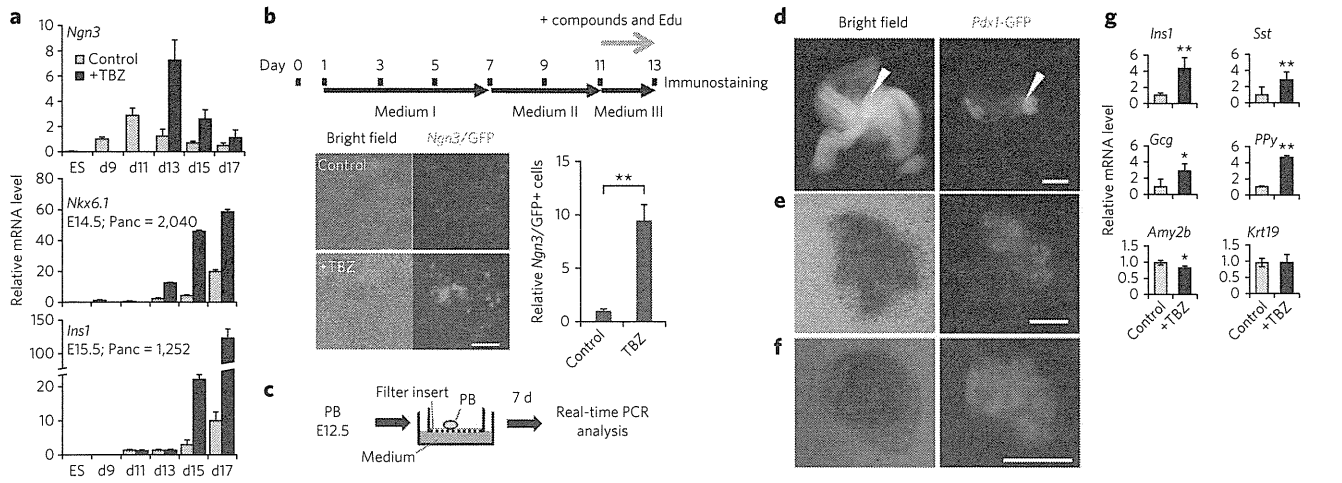

Figure 3 | VMAT2 inhibition increased differentiation into *Ngn3*-GFP+ cells. TBZ increased differentiation into *Ngn3*-GFP+ cells without increasing proliferation. (**a**) *Ngn3*, *Nkx6.1* and *Ins1* expression assayed on differentiation days (d) 13, 15 and 17, with or without (w/o) TBZ, expressed as fold change relative to control on day 13. Gray bars, no chemical (vehicle) samples; black bars, TBZ-treated samples. For all graphs, (n = 3). (**b**) A schematic drawing of the experimental design is shown. ES cell cultures were added with TBZ from day 11 to day 13 and assayed on day 13. Transmission or fluorescence images (left) and quantitative representations (right) of *Ngn3*-GFP+ cells without TBZ on day 13 are shown. (**c**) Schematic drawing of the experimental design. Pancreatic rudiments (PB, pancreatic bud) dissected from *Pdx1*-GFP mice at E12.5 were used for *ex vivo* culture for 7 d on filter inserts. (**d**–**f**) Transmission (left) and fluorescence (right) micrographs of explants before (**d**) and after culturing without TBZ (**e**; control DMSO) or with TBZ (**f**). (**g**) Semiquantitative real-time PCR was used to assay the expression of *Gcg*, *Sst*, *PPy*, *Amy2b* or *Krt19* after 7-d culture. Data shown are mean ± s.d. (n = 3), expressed as relative cell number compared to control. Scale bars, 200 μm. $^*P < 0.05$ and $^{**}P < 0.01$ (two-tailed paired Student's t-test).

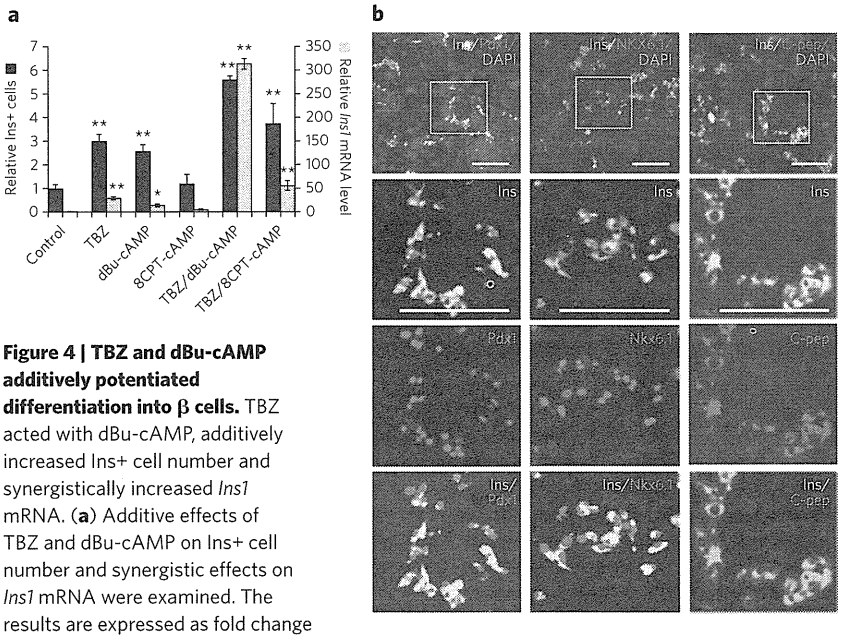

Figure 4 | TBZ and dBu-cAMP additively potentiated differentiation into β cells. TBZ acted with dBu-cAMP, additively increased Ins+ cell number and synergistically increased *Ins1* mRNA. (**a**) Additive effects of TBZ and dBu-cAMP on Ins+ cell number and synergistic effects on *Ins1* mRNA were examined. The results are expressed as fold change relative to control vehicle treatment (DMSO). By contrast, treatment with 8CPT-cAMP, a cAMP analog that specifically activates Epac2, showed no effects. Data shown are mean ± s.d. ($n = 3$), expressed as relative cell number compared to control (no chemical treatment). On the *y* axis, 1 = 0.3% Ins+ cells. (**b**) Total ES cell cultures were assayed by immunohistochemistry. Ins staining (yellow) completely overlapped with staining (red) of Pdx1, Nkx6.1 and C-peptide for *in vitro* differentiated ES cells treated on days 11–17 with TBZ and dBu-cAMP. Blue shows DAPI staining. Scale bars, 100 μm. Lower panels are enlarged pictures of the boxes in the top panels. $^*P < 0.05$ and $^{**}P < 0.01$ (two-tailed paired Student's *t*-test).

pancreatic bud explant culture (**Fig. 3c–g**). We observed a slight decrease in *Amy2b*-expressing exocrine cells but no effects on *Krt19*-expressing duct cells. These results therefore suggested that VMAT2-mediated inhibition of the progress from Pdx1+ pancreatic progenitors to Ngn3+ endocrine progenitors exists in both normal pancreatic endocrine development (**Fig. 3c–g**) and ES cell differentiation (**Fig. 3b**).

The combinatory effects of TBZ and dBu-cAMP addition

Dopamine, histamine and serotonin are considered to function through binding to their receptors. All dopamine, histamine and serotonin receptors are G protein–coupled receptors[22]. In our screen, dibutyryl adenosine 3′,5′-cAMP (dBu-CAMP), a cell-permeable cAMP analog, was identified as a compound to promote β-cell differentiation. We examined the effects of dBu-cAMP and its synergy with TBZ. TBZ or dBu-cAMP alone increased the number of Ins+ cells or the amount of *Ins1* transcript, respectively. Simultaneous addition of TBZ and dBu-cAMP caused an approximately 300-fold increase in *Ins1* transcript, which is approximately 30-fold or 15-fold the effect of single addition of TBZ or dBu-cAMP, respectively (**Fig. 4a**).

In the adult islets, cAMP is known to regulate the potentiation of insulin secretion by a protein kinase A (PKA)-dependent mechanism and a PKA-independent mechanism that involves the cAMP-binding protein Epac2 (ref. 23). As dBu-cAMP activates both pathways[24,25], we then tested a cell-permeable analog, 8CPT-cAMP, that specifically activates Epac2 but not PKA[26]. Ins+ cell number or *Ins1* gene expression did not increase with application of 8CPT-cAMP, and neither showed an additive effect after treatment with 8CPT-cAMP and TBZ. The results suggested that the potentiation of β-cell differentiation by the dBu-cAMP signaling pathway is not mediated through activation of Epac2 but possibly through PKA (**Fig. 4a**).

We then analyzed the differentiated ES cell–derived β cells generated by TBZ and dBu-cAMP treatment by immunocytochemistry. The Ins+ cells expressed Pdx1 and Nkx6.1, which are mature β cell markers. Almost all of the Pdx1+ cells were Ins+. Almost all Ins+ staining overlapped with C-peptide+ staining (**Fig. 4b**). Ins+ cells expressed Nkx2.2, Nkx6.1 and MafA (**Supplementary Fig. 6a**). We also observed *Dolichos biflorus* agglutinin (DBA)+ pancreatic duct cells but not amylase+ exocrine cells in the ES cell culture (**Supplementary Fig. 6b**). There were no qualitative differences in the expression of the above markers among cells treated with both TBZ and dBu-cAMP or each alone (**Supplementary Fig. 6a,b**). We examined whether the Ins+ cells also expressed other endocrine hormones. Although some Ins-single-positive cells, which do not express other endocrine hormones, exist (approximately 10%) in the culture, over 90% of the Ins+ cells were polyhormonal cells, in which glucagon, somatostatin and/or pancreatic polypeptide were also expressed with insulin (**Supplementary Fig. 6**).

As almost all of the Pdx1+ cells derived from ES cells treated with TBZ or dBu-cAMP expressed insulin at the late stage (day 17), which corresponded to the second phase of Pdx1 expression, where Ins is also coexpressed. (**Fig. 1a**), we purified ES cell–derived *Pdx1*-GFP+ cells by flow cytometry (**Fig. 5a,b**) to analyze the β cells with respect to insulin content, GSIS and mRNA expression (**Fig. 5c–e**). *Pdx1*-GFP+ β cells comprised 10.2% of the total cells recovered (**Fig. 5b**). TBZ alone increased C-peptide content to 10 μg per mg, which is approximately 60% of that in adult islets (**Fig. 5c**). However, TBZ did not promote differentiation into cells capable of GSIS (**Fig. 5d**). Isolated *Pdx1*-GFP+ cells treated with dBu-cAMP alone increased GSIS to 170 ng per mg protein per h, which is 42% of that in mature islets (**Fig. 5d**). However, in contrast to TBZ, dBu-cAMP did not increase C-peptide content on a per-protein level (**Fig. 5d**).

The recovery of C-peptide contents from total ES cell–derived cells treated with TBZ, dBu-cAMP or both compounds is summarized in **Supplementary Figure 7a**. ES cell–derived β cells with a C-peptide content equivalent of approximately 100 islets could be obtained from one 96-well plate. The C-peptide contents increased by approximately 5.7-fold or 2.7-fold through treatment with TBZ or dBu-cAMP alone, respectively, and to 8.1-fold through treatment with both compounds (on a per μg DNA basis). This result is consistent with the above result that TBZ and dBu-cAMP additively increased Ins+ cell number.

We also examined the time-dependent effects of the chemicals on GSIS. TBZ alone did not alter GSIS, but dBu-cAMP alone potentiated ES differentiation into Ins+ cells, showing the ability for GSIS from day 15 (**Supplementary Fig. 7b**). To further confirm that the effect of dBu-cAMP occurs through potentiation of differentiation into Ins+ cells, we treated ES cells with dBu-cAMP in different time windows, that is, from day 11 to day 15 or from day 11 to day 17, and then assayed for GSIS on day 17. Treatment with dBu-cAMP for a longer period (day 11 to day 17) significantly ($P < 0.01$) enhanced GSIS compared to those treated from day 11 to day 15 (**Supplementary Fig. 8**). Treatment with dBu-cAMP during the secretion assay significantly ($P < 0.01$) increased GSIS. Therefore, dBu-cAMP treatment potentiated differentiation into matured β cells and enhanced GSIS ability. The results

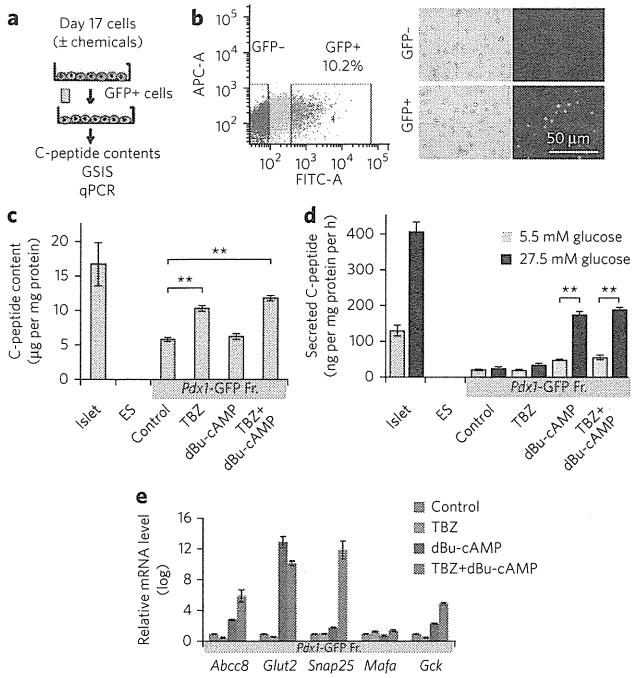

Figure 5 | Characterization of the purified ES cell-derived Ins+ and Pdx-GFP+ cells. TBZ and dBu-cAMP additively potentiated differentiation and maturation of ES cells into β cells with GSIS ability. (**a**–**e**) Differentiated β cells were purified by flow cytometry. Experimental procedures (**a**) and flow cytometry results (**b**) are shown. Cells were tested for their C-peptide contents (**c**), GSIS (**d**) and quantitative PCR (qPCR) (**e**). In **b**, *Pdx1*-GFP+ cells (10.2% of total cells) were purified by flow cytometry on the basis of GFP intensity. Scale bar, 50 μm. In **c** and **d**, treatment with TBZ alone increased C-peptide content, and treatment with dBu-cAMP alone evoked GSIS, as measured by C-peptide contents or secreted C-peptide with significant differences (two-tailed paired Student's *t*-test) $^{**}P < 0.01$. (**e**) Quantitative PCR was performed to quantify the expression of *Abcc8*, *Glut2*, *Snap25*, *Mafa* and *Gck*. In **c**–**e**, GFP+ cells from differentiated ES cells were used, to which DMSO (no chemical treatment), TBZ or dBu-cAMP or both (TBZ + dBu-cAMP) were added. In **c**, $n = 4$, and in **d** and **e**, $n = 3$.

showing that dBu-cAMP potentiated GSIS suggested that the enhancement of differentiation may be mediated by insulin. The effect of insulin was then examined by manipulating the insulin concentration in medium III (**Fig. 1a**), which contained 10 μM insulin in all of the experiments reported so far. Insulin potentiated the differentiation at 16 nM, and its effect declined with increasing insulin concentrations (**Supplementary Fig. 9**). Therefore, TBZ plus dBu-cAMP enhanced insulin secretion at low levels, which in turn accelerated the expression of *Ins1* and further drove β-cell differentiation.

Real-time PCR analyses revealed that dBu-cAMP administration alone increased the expression of genes implicated in GSIS: *Abcc8*, which encodes the regulatory sulfonylurea receptor SUR of the ATP-sensitive potassium channel, and the glucose transporter-encoding genes *Slc2a2* (also known as *Glut2*) and *Gck* (**Fig. 5e**). Double treatment with TBZ and dBu-cAMP upregulated expression of *Abcc8* and *Gck* by ~1×10^5-fold and upregulated expression of *Glut2* and *Snap25*, which encodes a component involved in the regulation of vesicular release, by ~1×10^{10}-fold compared to expression in the control (**Fig. 5e**).

Taken together, these results indicated that TBZ treatment increased insulin content and dBu-cAMP increased GSIS of the ES cell–derived cells. Simultaneous treatment with TBZ and dBu-cAMP enabled the ES cell–derived β cells to produce Ins and secrete Ins *in vitro* in a glucose-sensitive manner at levels comparable to that of adult islets.

The transplanted cells reversed hyperglycemia in mice

To examine their *in vivo* function, we transplanted ES cell–derived β cells into AKITA mice with immunodeficiency (*Rag1*$^{-/-}$ *Ins2*$^{Akita/+}$)[27]. The AKITA mouse is a model that inherits diabetes in a dominant manner owing to a missense mutation in *Ins2*. Consistent with our previous report[28], all male heterogeneous AKITA mice gradually developed hyperglycemia after they reached 6 weeks of age (**Supplementary Fig. 10a**). We harvested 4×10^6 or 1×10^7 ES cell–derived cells (treated with both TBZ and dBu-cAMP) on day 17 and grafted the cells under the kidney capsule in each experimental mouse. The experimental mice showed a reversal of hyperglycemia for more than 6 weeks, with larger grafts showing increasing effects (**Supplementary Fig. 10a**), whereas no change in blood glucose was observed in control untransplanted AKITA mice.

We then transplanted 1×10^7 ES cell–derived cells, which were treated with no chemical, TBZ or dBu-cAMP alone or with both TBZ and dBu-cAMP, into the kidney capsule of the AKITA mice. Mice engrafted with cells that were not treated with growth factors served as negative controls. Mice transplanted with cells treated with TBZ plus dBu-cAMP or dBu-cAMP alone partially recovered from hyperglycemia and showed lowered fasting blood glucose as early as 2 weeks after engraftment (**Fig. 6a**). Mice engrafted with cells treated with both TBZ and dBu-cAMP completely recovered from glucose intolerance, whereas those engrafted with cells treated with dBu-cAMP alone did not (**Fig. 6a–c**). In both cases, the engrafted mice showed even higher levels of plasma C-peptide compared to that in the control wild-type BL6 mice (**Supplementary Fig. 10b**). The AKITA mice are reported to be insulin resistant[29]. The above results might reflect the insulin resistance of the recipient AKITA mice. In contrast, mice engrafted with cells treated with TBZ alone responded to glucose administration and increased plasma C-peptide levels more rapidly compared to those engrafted with control cells (no chemical treatment) (**Supplementary Fig. 10b**), which agreed with their partial reversal of glucose tolerance (**Fig. 6b**) and fasting blood glucose (**Fig. 6a**).

Grafts without noticeable tumor formation were recovered from the experimental mice and were found to express insulin (**Supplementary Fig. 10c**). No insulin-positive cells coexpressed glucagon, pancreas polypeptide or somatostatin. We confirmed that the β-cell mass in the recipient AKITA pancreas did not increase after transplantation, showing an altered allocation of glucagon+ cells at the center of the islets, in contrast to their peripheral localization in the control wild-type mice (**Supplementary Fig. 10d**). Taken together, we concluded that the reversal of hyperglycemia and restoration of glucose tolerance was due to the transplanted ES cell–derived cells.

These results demonstrate that treatment of both TBZ and dBu-cAMP potentiated differentiation of ES cells into cells, with a high level of C-peptide contents and GSIS ability, and transplantation of these cells reversed hyperglycemia in AKITA diabetic mice.

DISCUSSION

Although the function of VMAT2 in the pancreas is largely unknown, VMAT2 is known to take up monoamines such as dopamine, histamine and serotonin into secretory granules of neurons and exert both autocrine and paracrine functions in the nervous system. VMAT2 is described to be expressed in human β cells. However, there has been some controversy in the literature about its presence in β cells of rodents[30]. Here, the target cells of the VMAT2 inhibitors are differentiating pancreatic progenitor cells. We revealed a new role of VMAT2 and monoamine-dependent suppression of differentiation from the pancreatic progenitor cells.

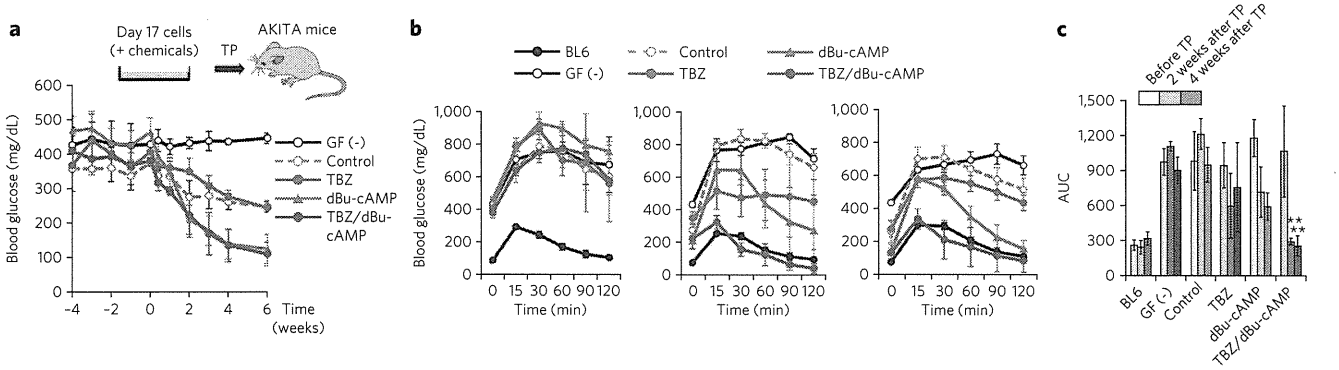

Figure 6 | Transplanted cells reversed hyperglycemia and glucose tolerance. Transplantation assays showed that the induced β cells normalized fasting blood glucose levels and glucose tolerance in the AKITA diabetic mice. (**a**) Top, experimental procedure. *In vitro* differentiated β cells, treated with TBZ and dBu-cAMP, were harvested on day 17 and transplanted into hyperglycemic AKITA mice. Bottom, fasting blood glucose levels (mg/dL) of mice transplanted with ES-derived β cells were measured before and after engraftment. X axis shows weeks after transplantation. (**b**) AKITA mice were analyzed for IPGTT before engraftment (left), 2 weeks (middle) or 4 weeks (right) after engraftment, and time courses of blood glucose levels (mg/dL) after challenge with glucose are shown. X axis shows minutes after glucose challenges. (**c**) Area under curve (AUC) of IPGTT curves shown in **b**. Light color bars, before engraftment; darker color bars, 2 weeks after engraftment; darkest color bars, 4 weeks after engraftment. In **a** and **b**, blue circles represent treatment with TBZ, green circles represent treatment with dBu-cAMP, purple circles represent treatment with TBZ and dBu-cAMP, broken lines with open circles represent no chemical treatment at 1×10^7, and black lines with open circles represent cells with no growth factor treatment (negative controls). In **a**–**c**, the significant differences between treatment and control were $^*P < 0.05$ or $^{**}P < 0.01$ (two-tailed unpaired Student's *t*-test) and are indicated above error bars, which show s.d.

Dopamine, histamine and serotonin are synthesized and stored in the endocrine pancreas during pregnancy[31] and in adult β cells[19]. In the adult, there are several lines of evidence supporting that dopamine and histamine negatively regulate insulin content, glucose tolerance[32–34] and GSIS[35–37]. In contrast, serotonin is reported to drive β-cell replication and regulate glucose tolerance in pregnant mice. However, the role of monoamines during embryonic development remains largely unknown.

Among the monoamines, dopamine is produced at a highest level in ES cell–derived cells and during embryonic stages. Consistent with this, dopamine synthesizing enzyme (encoded by *Th*), was expressed in the ES-derived cells at a level comparable to that in the embryonic pancreas. In spite of the differences in their cellular contents, inhibition of all three synthesizing enzymes showed similar effects to enhance β-cell differentiation, indicating that all of these monoamines take part in this process. It was puzzling that application of these monoamines dose-dependently suppressed β cell differentiation with similar EC_{50} values, although their EC_{50} against their specific receptors are very different[38–40]. We hypothesize that this is due to the fact that monoamine is taken up into the storage vesicles and their subsequent release is required for their action and that other components co-released from the vesicle might be required to convey their function[41].

Our results indicated that monoamines controlled by VMAT2 serve as a brake for differentiation of Pdx1+ pancreatic progenitors into Ngn3+ endocrine precursors and subsequently into Ins+ cells. Once this brake is released, the Pdx1+ cells are induced to differentiate into Ngn3+ cells, which quickly turn into Ins+ cells. TBZ acted during a short time window to increase Ngn3+ cells, suggesting that this brake functions transiently. However, whether there are specific roles for each of the monoamines remains an open question.

In the adult β cells, GLP1 and GIP are well known to activate $G\alpha_s$-coupled receptors and potentiate GSIS by activating cAMP signaling and modulating K_{ATP} channel activity. It is reported that cAMP signaling induces glucose responsiveness through both PKA and Epac2 dependent pathway[23]. PKA is reported to modulate VMAT2 by regulating its trafficking[42]. It is possible that cAMP activates β-cell differentiation through modulating VMAT2. It remains unknown whether GLP1, GIP or other unknown ligands function to promote the maturation of β cells to initiate GSIS during embryonic development. This would agree with the observation that pancreas-specific $G\alpha_s$-deficient mice demonstrated reduced β-cell mass and defects in glucose response[43].

Most of the ES cell–derived insulin+ cells were polyhormonal cells, coexpressing other endocrine hormones. Maturation rapidly occurred *in vivo*. They rapidly turned into insulin-single positive cells after they were grafted under kidney capsules. Intrapenitoneal glucose trelant test (IPGTT) results revealed that cells doubly treated with TBZ and dBu-cAMP matured into cells capable of GSIS and restored glucose tolerance as early as 2 weeks after engraftment. Cells treated with TBZ alone or with no chemicals also matured *in vivo* and became potent for GSIS within 2 weeks. In mouse pancreatic development, Ins+ glucagon+ cells appear early in 'first transition', and they do not contribute to the generation of mature β cells[44]. These cells do not express mature endocrine markers[45]. By contrast, Ins+ glucagon+ transitional cells exist transiently during the conversion of α cells into β cells[46,47]. The polyhormonal cells observed in the present study expressed mature endocrine markers. Therefore, the ES cell–derived polyhormonal cells here might have characteristics close to the transitional cells that appear during cell fate conversion rather than those that exist during early mouse embryonic development. Although the exact mechanism of how ES cells mature under *in vivo* environment remains unknown, it is reported that dynamic chromatin remodeling occurs in human ES cells after they are engrafted *in vivo*[48]. Previous studies have shown that human ES cell–derived insulin-expressing cells, which are polyhormonal, differentiate into α cells, instead of β cells, after transplantation[49]. The discrepancies might be due to the differences in the underlying mechanism between the mouse and human ES cells or due to the differences between the culture protocols. However, it is technically difficult for us to perform further long-term analyses, such as transplantation or re-culture of the mouse ES cell–derived Pdx1/GFP+ cells, owing to a significant ($P < 0.01$) loss of cell viability after sorting at this late stage of differentiation. Taken together, although we cannot completely rule out other possibilities, our results suggested that the transplanted insulin-expressing cells reversed hyperglycemia in AKITA mice.

The graft experiments showed that transplanting 4×10^6 or 1×10^7 ES cell–derived cells, with their C-peptide contents equivalent to 40 or 100 islets, respectively, is enough to reverse hyperglycemia in AKITA diabetic mice. This is lower than the previously reported observation that it is necessary to transplant 150–200 islets to reverse hyperglycemia[50]. Our results suggested that these ES cell–derived cells rapidly underwent further differentiation *in vivo* and increased their C-peptide contents or GSIS ability so that a lower number of ES cell–derived cells was enough for the reversal of hyperglycemia.

The ES cell–derived cells showed no signs of tumor formation. This might due to the high differentiation efficiency into the definitive endoderm. Moreover, the long differentiation period might also result in a low population of undifferentiated cells remaining in culture.

In conclusion, results of the present study demonstrated a previously unknown function of VMAT2 in controlling differentiation into pancreatic endocrine precursors. VMAT2 inhibition and dBu-cAMP addition synergized and further increased *Ins1* transcripts and are sufficient to promote differentiation of ES cells into functional β cells capable of reversing hyperglycemia in diabetic mice. Future studies would be required to analyze the role of VMAT2 during human induced pluripotent stem cell cell differentiation to apply this protocol for future cell replacement therapy.

Received 15 December 2012; accepted 15 October 2013; published online 15 December 2013

METHODS

Methods and any associated references are available in the online version of the paper.

References

1. Jonsson, J., Carlsson, L., Edlund, T. & Edlund, H. Insulin-promoter-factor 1 is required for pancreas development in mice. *Nature* **371**, 606–609 (1994).
2. Gu, G., Dubauskaite, J. & Melton, D.A. Direct evidence for the pancreatic lineage: NGN3+ cells are islet progenitors and are distinct from duct progenitors. *Development* **129**, 2447–2457 (2002).
3. Gradwohl, G., Dierich, A., LeMeur, M. & Guillemot, F. *neurogenin3* is required for the development of the four endocrine cell lineages of the pancreas. *Proc. Natl. Acad. Sci. USA* **97**, 1607–1611 (2000).
4. Puri, S. & Hebrok, M. Cellular plasticity within the pancreas—lessons learned from development. *Dev. Cell* **18**, 342–356 (2010).
5. D'Amour, K.A. *et al.* Efficient differentiation of human embryonic stem cells to definitive endoderm. *Nat. Biotechnol.* **23**, 1534–1541 (2005).
6. Skoudy, A. *et al.* Transforming growth factor (TGF)β, fibroblast growth factor (FGF) and retinoid signalling pathways promote pancreatic exocrine gene expression in mouse embryonic stem cells. *Biochem. J.* **379**, 749–756 (2004).
7. D'Amour, K.A. *et al.* Production of pancreatic hormone-expressing endocrine cells from human embryonic stem cells. *Nat. Biotechnol.* **24**, 1392–1401 (2006).
8. Borowiak, M. *et al.* Small molecules efficiently direct endodermal differentiation of mouse and human embryonic stem cells. *Cell Stem Cell* **4**, 348–358 (2009).
9. Chen, S. *et al.* A small molecule that directs differentiation of human ESCs into the pancreatic lineage. *Nat. Chem. Biol.* **5**, 258–265 (2009).
10. Shiraki, N. *et al.* Guided differentiation of embryonic stem cells into Pdx1-expressing regional-specific definitive endoderm. *Stem Cells* **26**, 874–885 (2008).
11. Higuchi, Y. *et al.* Synthesized basement membranes direct the differentiation of mouse embryonic stem cells into pancreatic lineages. *J. Cell Sci.* **123**, 2733–2742 (2010).
12. Wang, Y.M. *et al.* Knockout of the vesicular monoamine transporter 2 gene results in neonatal death and supersensitivity to cocaine and amphetamine. *Neuron* **19**, 1285–1296 (1997).
13. Pothos, E.N. *et al.* Synaptic vesicle transporter expression regulates vesicle phenotype and quantal size. *J. Neurosci.* **20**, 7297–7306 (2000).
14. Vergo, S., Johansen, J.L., Leist, M. & Lotharius, J. Vesicular monoamine transporter 2 regulates the sensitivity of rat dopaminergic neurons to disturbed cytosolic dopamine levels. *Brain Res.* **1185**, 18–32 (2007).
15. Eiden, L.E. & Weihe, E. VMAT2: a dynamic regulator of brain monoaminergic neuronal function interacting with drugs of abuse. *Ann. NY Acad. Sci.* **1216**, 86–98 (2011).
16. Erickson, J.D., Schafer, M.K., Bonner, T.I., Eiden, L.E. & Weihe, E. Distinct pharmacological properties and distribution in neurons and endocrine cells of two isoforms of the human vesicular monoamine transporter. *Proc. Natl. Acad. Sci. USA* **93**, 5166–5171 (1996).
17. Anlauf, M. *et al.* Expression of the two isoforms of the vesicular monoamine transporter (VMAT1 and VMAT2) in the endocrine pancreas and pancreatic endocrine tumors. *J. Histochem. Cytochem.* **51**, 1027–1040 (2003).
18. Simpson, N.R. *et al.* Visualizing pancreatic β-cell mass with [^{11}C]DTBZ. *Nucl. Med. Biol.* **33**, 855–864 (2006).
19. Saisho, Y. *et al.* Relationship between pancreatic vesicular monoamine transporter 2 (VMAT2) and insulin expression in human pancreas. *J. Mol. Histol.* **39**, 543–551 (2008).
20. Grimsby, J., Chen, K., Wang, L.J., Lan, N.C. & Shih, J.C. Human monoamine oxidase A and B genes exhibit identical exon-intron organization. *Proc. Natl. Acad. Sci. USA* **88**, 3637–3641 (1991).
21. Gu, G. *et al.* Global expression analysis of gene regulatory pathways during endocrine pancreatic development. *Development* **131**, 165–179 (2004).
22. Kroeze, W.K., Sheffler, D.J. & Roth, B.L. G-protein-coupled receptors at a glance. *J. Cell Sci.* **116**, 4867–4869 (2003).
23. Seino, S., Shibasaki, T. & Minami, K. Dynamics of insulin secretion and the clinical implications for obesity and diabetes. *J. Clin. Invest.* **121**, 2118–2125 (2011).
24. Lo, K.W., Kan, H.M., Ashe, K.M. & Laurencin, C.T. The small molecule PKA-specific cyclic AMP analogue as an inducer of osteoblast-like cells differentiation and mineralization. *J. Tissue Eng. Regen. Med.* **6**, 40–48 (2012).
25. Mei, F.C. *et al.* Differential signaling of cyclic AMP: opposing effects of exchange protein directly activated by cyclic AMP and cAMP-dependent protein kinase on protein kinase B activation. *J. Biol. Chem.* **277**, 11497–11504 (2002).
26. Kelley, G.G. *et al.* Glucose-dependent potentiation of mouse islet insulin secretion by Epac activator 8-pCPT-2′-O-Me-cAMP-AM. *Islets* **1**, 260–265 (2009).
27. Wang, J. *et al.* A mutation in the insulin 2 gene induces diabetes with severe pancreatic β-cell dysfunction in the *Mody* mouse. *J. Clin. Invest.* **103**, 27–37 (1999).
28. Mochida, T. *et al.* Time-dependent changes in the plasma amino acid concentration in diabetes mellitus. *Mol. Genet. Metab.* **103**, 406–409 (2011).
29. Hong, E.G. *et al.* Nonobese, insulin-deficient Ins2Akita mice develop type 2 diabetes phenotypes including insulin resistance and cardiac remodeling. *Am. J. Physiol. Endocrinol. Metab.* **293**, E1687–E1696 (2007).
30. Schäfer, M.K. *et al.* Species-specific vesicular monoamine transporter 2 (VMAT2) expression in mammalian pancreatic β cells: implications for optimising radioligand-based human β cell mass (BCM) imaging in animal models. *Diabetologia* **56**, 1047–1056 (2013).
31. Harris, P.E. *et al.* VMAT2 gene expression and function as it applies to imaging β-cell mass. *J. Mol. Med.* **86**, 5–16 (2008).
32. Fülöp, A.K. *et al.* Hyperleptinemia, visceral adiposity, and decreased glucose tolerance in mice with a targeted disruption of the histidine decarboxylase gene. *Endocrinology* **144**, 4306–4314 (2003).
33. Buchanan, T.A. & Xiang, A.H. Gestational diabetes mellitus. *J. Clin. Invest.* **115**, 485–491 (2005).
34. Kim, H. *et al.* Serotonin regulates pancreatic β cell mass during pregnancy. *Nat. Med.* **16**, 804–808 (2010).
35. Rubí, B. *et al.* Dopamine D2-like receptors are expressed in pancreatic β cells and mediate inhibition of insulin secretion. *J. Biol. Chem.* **280**, 36824–36832 (2005).
36. Ericson, L.E., Hakanson, R. & Lundquist, I. Accumulation of dopamine in mouse pancreatic B-cells following injection of l-DOPA. Localization to secretory granules and inhibition of insulin secretion. *Diabetologia* **13**, 117–124 (1977).
37. Zern, R.T., Bird, J.L. & Feldman, J.M. Effect of increased pancreatic islet norepinephrine, dopamine and serotonin concentration on insulin secretion in the golden hamster. *Diabetologia* **18**, 341–346 (1980).
38. Seeman, P. *et al.* The dopaminergic stabilizer ASP2314/ACR16 selectively interacts with $D2^{High}$ receptors. *Synapse* **63**, 930–934 (2009).
39. Braden, M.R., Parrish, J.C., Naylor, J.C. & Nichols, D.E. Molecular interaction of serotonin 5-HT2A receptor residues $Phe339^{(6.51)}$ and $Phe340^{(6.52)}$ with superpotent *N*-benzyl phenethylamine agonists. *Mol. Pharmacol.* **70**, 1956–1964 (2006).
40. Peakman, M.C. & Hill, S.J. Endogenous expression of histamine H1 receptors functionally coupled to phosphoinositide hydrolysis in C6 glioma cells: regulation by cyclic AMP. *Br. J. Pharmacol.* **113**, 1554–1560 (1994).
41. El Mestikawy, S., Wallen-Mackenzie, A., Fortin, G.M., Descarries, L. & Trudeau, L.E. From glutamate co-release to vesicular synergy: vesicular glutamate transporters. *Nat. Rev. Neurosci.* **12**, 204–216 (2011).
42. Yao, J., Erickson, J.D. & Hersh, L.B. Protein kinase A affects trafficking of the vesicular monoamine transporters in PC12 cells. *Traffic* **5**, 1006–1016 (2004).
43. Xie, T., Chen, M. & Weinstein, L.S. Pancreas-specific Gs_α deficiency has divergent effects on pancreatic α- and β-cell proliferation. *J. Endocrinol.* **206**, 261–269 (2010).